Anoxic Alkaline Oxidation of Bisulfide by Fe/Ce Oxides: Reaction Pathway

Catalin F. Petre and Faïçal Larachi
Dept. of Chemical Engineering, Laval University, QC, Canada G1K 7P4

DOI 10.1002/aic.11241
Published online July 3, 2007 in Wiley InterScience (www.interscience.wiley.com).

The kinetics of the anoxic reaction between bisulfide and iron/cerium oxide–hydroxide was studied for alkaline pH [8.0–11.0] at 0.1 MPa and 298 K in a batch slurry reactor as a part and parcel of the surface chemistry in action in the oxidation of the total reduced sulfur pollutants in the pulp and paper atmospheric emissions. Bisulfide was converted into thiosulfate and polysulfides; while the leached divalent iron and thiosulfate dovetailed equimolarly for pH $\geq$ 9.5 which was attributed to the breaking of sulfur–oxygen surface intermediates initiated by iron-disulfide $Fe^{II}(SS)$ complexes. X-ray photoelectron spectroscopy of S 2p and Fe 2p of the material revealed iron sulfide, polysulfides/elemental sulfur and thiosulfate signatures along with Fe(III) oxide–hydroxide, Fe(II) sulfide and some Fe(II) connected to sulfoxy species. A detailed reaction pathway of the anoxic oxidation of bisulfide by Fe/Ce oxide–hydroxide based on $Fe^{II}(SS)$ complex was proposed for explaining the formation of zerovalent sulfur, thiosulfate, and leached ferrous iron, and whereof a kinetic model was derived to depict the Fe(II) leaching and bisulfide consumption rates. The model rate constants were analyzed in terms of sensitivity to pH, and initial concentrations of bisulfide and surface Fe(III). *AIChE J,* 53: 2170–2187, 2007
Keywords: pulp and paper emissions, sulfur abatement, pathway and kinetic model, XPS characterization, bisulfide oxidation, iron/cerium oxide-hydroxide, thiosulfate, polysulfides

Introduction

A great deal of pulping mills exploits chemical pulping to enhance delignification of wood chips to free the more valuable (hemi)cellulose-rich fibers.[1] The kraft process, wherein sodium sulfide is a key constituent of the cooking liquor, is responsible for the emission of malodorous chemically reduced thiocompounds known as total reduced sulfurs (or TRS). TRS gases refer specifically to the quartet: hydrogen sulfide (H_2S), methyl mercaptan (CH_3SH), dimethyl sulfide (CH_3SCH_3), and dimethyl disulfide ($CH_3S_2CH_3$). Such objectionable pollutants leap out of point source equipments in use for chemical and black liquor recovery, such as in lime kilns or recovery furnaces, which emit low-volume high-concentration (LVHC) streams with up to 1000 ppmv TRS load, or for pulp production such as digesters and brownstock washers which generate the so-called high-volume low-concentration (HVLC) emissions containing up to 200 ppmv TRS. These levels are 40–200 times above the regulated emission levels while exceeding by at least two orders of magnitude the human odor threshold, about 1–10 ppbv. Such high sensitivity of human olfactory system towards minute TRS levels, especially in populated areas neighboring pulping mills, exposes this industry to stiff environmental scrutiny. Since the early 1990's matter-of-factly, Canada and the United States[2] have been enforcing regulatory measures targeting the kraft pulp manufacturers to collect and treat all their plant vents involved in belching TRS in the atmosphere.[3]

Correspondence concerning this article should be addressed to F. Larachi at faical.larachi@gch.ulaval.ca.

Several TRS abatement processes have been advocated such as alkaline/amine scrubbing and gas incineration,[4,5] chemical oxidation by NaClO, ClO_2, H_2O_2, $KMnO_4$, and gas phase oxidation by ClO_2,[6] aminal scavenging,[7,8] wet oxidation,[9,10] aerobic biofiltration,[11,12] activated carbon, and green liquor dregs adsorption.[13,14] Only incineration and alkaline scrubbing are nowadays massively implemented industrially. However, capital and operating costs of incineration remain prohibitive due not only to the high temperatures required (>600°C) but also to the installation of downstream scrubbers to intercept the epiphenomenal SO_x belching from the incinerator. Alkaline/amine scrubbing on the other hand is used as a complement, seldom as an alternative, to combustion for completing the removal of TRS, let alone that conventional scrubbing cannot get rid of the four TRS pollutants altogether, specifically CH_3SCH_3 and $CH_3S_2CH_3$. Though chemical oxidation by means of bleaching agents available in kraft plants leads to high TRS conversions, it suffers poor selectivity as costly oxidant is consumed in nonspecific attacks of non-TRS compounds, such as turpentine and methanol, present within the HVLC/LVHC streams. Aminal scavenging would entail extra costs because the required amine–aldehyde molecules are not available on site. Besides being costly, odor scavengers exhibit in addition limited lifetime and require usage at large excess with respect to the pollutant. Activated carbon alkaline slurries demonstrated limited adsorptive capacities setting aside this process considering the important effluent volumes and TRS levels in play. Wet oxidation of TRS is capital and energy intensive with regard to the process requirements (>100°C and ≥1 MPa)[15] which are incompatible with the lenient (P,T) conditions defining TRS effluents. An additional limitation of wet oxidation resides in its inability to deeply mineralize organic sulfur.[10] Aerobic biofiltration by means of peat or acclimated compost is barely conceivable in regard to the severe pressure drops across the randomly packed biofilter beds, high gas flow rates would bring about. In addition, the modest productivities achieved by the sulfide selective microorganisms (<1 g sulfur removal/day/kg bed) would require phenomenal peat or compost quantities to achieve sufficient bioreactor residence times.

This succinct survey reveals that efficient and economically viable TRS abatement methods are virtually nonexistent because of reagent and/or capital and operating costs. New processes aiming at odor-free kraft mill atmospheric emissions are still needed to respond to the increasingly stringent legislations, not to mention that a versatile process treating indistinctively the four TRS altogether remains yet to be invented. A convenient solution would be to intercept the gaseous TRS which are thence converted into retrievable sulfur, e.g., in the form of polysulfides, for reuse in the process while requiring little amounts of a fully regenerable oxidizing agent.

An alternative approach to oxidize TRS would exploit the iron redox chemistry in aqueous media as practiced for decades in the natural gas and oil refining industries for hydrocarbon desulfurization, e.g., LO-CAT, MEROX, Sulfint or SulFerox processes.[16–18] Notwithstanding, a key distinction reflects in the concomitant pairing of dioxygen with TRS in the kraft mill atmospheric effluents, the hydrocarbon streams are deprived of. This has profound implication on a scrubbing technology tailored for TRS removal where the simultaneous presence of aqueous-dissolved molecular oxygen can regenerate in situ the Fe(II) into the active Fe(III).

Hence, a simple redox scrubbing concept for treating hydrogen sulfide and methyl mercaptan contaminated air stream at ambient conditions has been recently evaluated which consists in oxidizing the pollutant, after being scrubbed in a mildly alkaline solution (pH ≈ 8–11), by means of powdered iron/cerium oxides–hydroxides.[19,20] This concept takes advantage of the association within the kraft mill HVLC/LVHC streams of plentiful oxygen that can be used for perpetuating the pollutant conversion through the oxidative regeneration of iron active sites. The global reaction is evocative of a pseudo-catalytic system consisting of two antagonistic stoichiometric processes that could be run simultaneously within one single reactor unit: on the one hand, oxidation of H_2S (and/or methyl mercaptan), more precisely its bisulfide companion HS^- (and/or methyl mercaptide, CH_3S^-), via reduction of ferric iron sites; on the other hand, an oxygen-mediated reoxidation of ferrous iron sites. Association of cerium to iron was shown to give rise to more accessible reaction sites, while availability of O_2 boosted significantly both the bisulfide and methyl mercaptide conversions.[19,20]

Despite the mechanism and kinetics of the reaction between Fe oxides–hydroxides and dissolved sulfide have been the subject of numerous studies, comprehension of this reaction is still fragmentary.[21–27] All the previous studies were carried out specifically at moderately acidic to neutral pH conditions, which are reminiscent of those conditions encountered during the reactive dissolution of iron oxides–hydroxides within sulfidic natural water environments, e.g., sediments and euxinic basins.[21–28] These studies concluded that the roles of oxide surface area, dissolved sulfide concentration, and pH are influential with regard to the reaction kinetics. Notwithstanding, the chemistry of the HS^-/Fe(III) surface leaching reaction for the conditions of interest to the process being explored for TRS abatement in kraft pulping, lacks scientific data, and remains largely undocumented within the alkaline pH region whereupon the scrubbing application is to be sought.

In a previous work,[29] the authors studied the initial rates of bisulfide oxidation and iron (Fe^{2+}) dissolution for the reaction between bisulfide and iron/cerium oxide–hydroxide under inert N_2 atmosphere in a mechanically stirred slurry reactor. The main observation stemming from that study was that bisulfide oxidation by iron/cerium oxide–hydroxide was controlled by the formation of surface bisulfide complexes and by the availability of Fe(III) reactive surface sites. The rate of bisulfide oxidation was ~10 times faster than the rate of iron dissolution. Anoxic oxidation of bisulfide by means of Fe/Ce oxide–hydroxide led to thiosulfate and zerovalent sulfur.[29]

The formation mechanism of thiosulfate, polysulfides and dissolved iron is important to an in-depth understanding of the reactions that take place in the poorly investigated high pH-region (pH ≈ 8–11).[29] All previous literature studies[21–29] reported almost unanimously two types of reaction products for the reaction between bisulfide and iron oxides–hydroxides. The first one is zerovalent sulfur[23–27,29] (suggested to be colloidal sulfur or both colloidal sulfur and polysulfides),

while the second corresponds to sulfoxy species, predominantly sulfate[23–26] or thiosulfate.[21,29]

The reaction between iron oxides–hydroxides and dissolved bisulfide has been suggested to proceed via the following sequence of elementary steps[23]:

(I) Formation of iron–sulfur surface complex

$$[Fe^{III}(OH)] + (HS^-) \rightarrow [Fe^{III}(S)^-] + H_2O \quad (R1)$$

(II) Electron transfer and conversion to divalent iron

$$[Fe^{III}(S)^-] \rightarrow [Fe^{II}(S)] \quad (R2)$$

(III) Release of oxidized sulfur product

$$[Fe^{II}(S)] + (H_2O) \rightarrow [Fe^{II}(OH_2)^+] + (S^{-\bullet}) \quad (R3)$$

(IV) Detachment of Fe(II)

$$[Fe^{II}(OH_2)^+] + H^+ \rightarrow Fe^{2+} + H_2O + [*], \quad (R4)$$

where $[*]$ represents a new surface site.

The surface complex formation (R1) is generally assumed to occur rapidly at the oxide surface, followed by electron transfer (R2).[27] In the case of bisulfide oxidation by ferrihydrite and goethite, the final oxidized product is predominantly elemental sulfur (R5):[22,25–27]

$$8[Fe^{III}(OH)] + 8S^{-\bullet} \rightarrow 8\,Fe^{2+} + S_8^0 \quad (R5)$$

In the case of hematite and lepidocrocite, the final oxidation product was sulfate (R6):[23,24]

$$7[Fe^{III}(OH)] + S^{-\bullet} \rightarrow 7\,Fe^{2+} + SO_4^{2-} \quad (R6)$$

In addition, the released Fe^{2+} may react with dissolved bisulfide to ultimately yield solid FeS (R7)[27]:

$$Fe^{2+} + HS^- + OH^- \rightarrow [FeS] + H_2O \quad (R7)$$

The stoichiometric coefficient values "8" and "7" in (R5) and (R6) indicate that these are not elementary steps and that the mechanism of bisulfide oxidation by iron oxides–hydroxides is still ambiguous and not fully understood. Questions that still deserve answers concern (i) which route yields to the formation of elemental sulfur? (ii) What could be the role played by polysulfides in the leaching reaction of iron? (iii) And how can the formation of sulfoxy species (sulfate and/or thiosulfate) be explained in anoxic conditions?

Of the global picture of the chemistry between TRS and iron relevant to the process, the present study will specifically address the interactions between bisulfide and iron at the mild alkaline pH values [8.0–11.0] characteristic of the TRS bifunctional process and in the absence of dissolved molecular oxygen. It has three main aims:

1. Contribute for an elucidation of the reaction mechanism for the formation of polysulfides, thiosulfate and dissolved iron in alkaline pH conditions.

2. Assess the influence of bisulfide oxidation products on the reaction mechanism and kinetics.

3. Develop a reaction pathway and a kinetic model to depict the fate of bisulfide oxidation, iron dissolution, and the formation of the oxidation products thereof.

Experimental Section

Fe/Ce oxide–hydroxide: preparation and characterization

All materials were ACS grade and all solutions were prepared with distilled water. A modified co-precipitation protocol was used to synthesize the Fe/Ce composite oxide–hydroxide (Fe/CeOx) with a mole ratio Fe/Ce of 9/1. Iron content was verified using an atomic absorption spectroscopy technique with a Perkin-Elmer AAnalyst 800.[19,29] The material was calcined in air at 300°C for 3 h and yielded an average specific surface area of 100 m^2/g (multipoint BET method, Micrometrics TRISTAR 3000 analyzer). This synthesis method led to an amorphous material as confirmed from the X-ray diffractograms performed on a Siemens D5000 diffractometer using the Cu-K_α radiation at 40 kV and 30 mA (λ = 1.54184 Å) at 1°/min [2θ].

X-ray photoelectron spectra were acquired at room temperature on an AXIS ULTRA X-ray photoelectron spectrometer from Kratos Analytical using a monochromatic Al-K_α (hv = 1486.6 eV) X-ray source operated at 300 W. The photoelectron kinetic energies were measured using a hemispherical electrostatic analyzer working in a constant pass energy mode. Survey scans (0–1150 eV) and high-resolution spectra of C 1s, O 1s, S 2p, and Fe 2p were acquired at pass energies of 160 and 20 eV, respectively, which correspond to energy step sizes of 1 eV and 50 meV, respectively. As the charge effects were expected to occur during the XPS analyses of the (poorly conducting) Fe/Ce oxide-hydroxide, the binding energy of the C 1s core level from adventitious carbon at 284.5 ± 0.1 eV was used as a reference to calibrate the high-resolution spectra. An extensive literature of reference values for binding energies (BE) for the relevant species (Fe, S, and O) is given in Table 1. The recorded spectra were decomposed by curve fitting synthetic peak components using the software package CasaXPS® (computer aided surface analysis for X-ray photoelectron spectroscopy; Casa Software, UK) by means of Gaussian-Lorentzian mixed peak shapes for both S 2p and O 1s core level spectra. The S 2p peaks were fitted using 2p1/2 and 2p3/2 doublets of typically 1.4 eV in width (fwhm), separated by a spin-orbit splitting of 1.18 eV and the S 2p1/2 peak area was constrained to one-half of the area of the S 2p3/2 peak area.

Reaction setup

Temperature-controlled (25°C) reactions between Fe/Ce oxide–hydroxide and bisulfide were carried out at different pH values (8.0–11.0) in a 1.5 L (300 mL of liquid) batch, sealed, double-jacketed, and magnetically stirred glass reactor under inert head-space (N_2 atmosphere). The pH was measured using an Oakton 1000 series pH-meter with a precision of ±0.01. The initial dissolved bisulfide concentration range was of 0.35–3.30 mmol/L and the initial Fe/Ce oxide–hydroxide surface area varied between 16 and 143 m^2/L. The particles ensemble-average diameter was measured to be 35 μm using an optical microscope. The absence of dissolved oxygen—usually maintained <0.1 ppm—was verified using a dissolved oxygen probe (DOB-930 model from Omega). The pH was held constant using a prepared 100 mmol/L borate buffer (Sigma-Aldrich) adjusted to the desired pH with

Table 1. XPS-Binding Energies Reported in the Literature for the Chemical Species Relevant to the Present Study (S, Fe, and O)

No.	Species	Binding Energy (eV)	Material	Reference
Fe 2p3/2				
1	$Fe^{(II)}$—S	706.7–707.5	–	34–43
2		708.5	Pyrrhotite ($Fe_{0.89}S$)	36
3		707.5–707.8	Pyrrhotite (Fe_7S_8)	37,41,44
4		707.3	Greigite (Fe_2^{3+}, $Fe^{2+}S_4$)	45
5		707.8	Mackinawite ($Fe_{1+x}S$)	46
6		707.1–707.5	Pyrite (FeS_2)	47,48
7		711.0	$FeSO_4$	48
8	$Fe^{(III)}$—S	708.9–709.3	Pyrrhotite (Fe_7S_8)	41,44
9		709.2	Greigite (Fe_2^{3+}, $Fe^{2+}S_4$)	45
10		713.3	$Fe_2(SO_4)_3$	48
11	Surface defects	708.8–709.2	–	40,41,43
12	$Fe^{(II)}$—O	709.5–709.9	–	48–50
13	($Fe_2^{(III)}$, $Fe^{(II)}$)—O	710.2–710.8	Magnetite (Fe_3O_4)	48,49
14	$Fe^{(III)}$—O	710.2–711.3	Hematite (α-Fe_2O_3)	48–55
15		710.8–712.9	Goethite (α-FeOOH)	43,50,54,55
S 2p				
16	S^{2-}	160.1–162.4	–	34,37,41,47
17		161.2	Pyrrhotite (Fe_7S_8)	44
18	S_2^{2-}	162.3–162.5	–	34,38,41–43
19		162.1–162.8	Pyrite (FeS_2)	38,44,47,56,57
20		162.0–162.4	Mackinawite ($Fe_{1+x}S$)	46,48
21		161.3–161.4	Pyrrhotite (Fe_7S_8)	37,41,44
22		161.6	Pyrrhotite ($Fe_{0.89}S$)	36
23		161.0	Greigite (Fe_2^{3+}, $Fe^{2+}S_4$)	45
24	S_4^{2-}	162.0–163.0	$[Cu^{I}(S_4)_3]^{3-}$	57,58
25	S_5^{2-}	161.9–163.2	$[Pt^{IV}(S_5)_3]^{2-}$	57,58
26	S_n^{2-}	163.3–165.3	–	41,44,59,60
27	S_8^0	163.6–164.4	–	38,43,44,48,57,60–62
28		163.8	Solid sulfur	This study
29	SO_3^{2-}	166.4–166.5	Na_2SO_3	44,60
30	SO_4^{2}	168.3–169.1	Na_2SO_4	37,41,44,45,47,60
31	$S_2O_3^{2-}$	161.8–163.0 (1st S)	$Na_2S_2O_3$	44,18,63
32		167.8–169.7 (2nd S)	$Na_2S_2O_3$	48,63
33		161.3 (1st S)	$Na_2S_2O_3$	This study
34		167.3 (2nd S)	$Na_2S_2O_3$	This study
O 1s				
35	Oxide	529.5–530.3	α-FeOOH	43,48,50,54,55
36		529.8–529.9	α-Fe_2O_3	49,50
37	Hydroxide	530.5–532.1	α-FeOOH	43,48,50,53,55
38		531.4	α-Fe_2O_3	49
39	Molecular water	531.5–533.8	α-FeOOH	37,43,48,53

NaOH (Fisher Scientific). Before the reaction was triggered, nitrogen (very high purity, Praxair Canada) was sparged through a fritted bubble distributor for 15 min throughout the aqueous solution to eliminate residual oxygen prior to sodium sulfide addition. The bisulfide precursor was $Na_2S \times 9H_2O$ salt (Sigma-Aldrich). The Na_2S salt crystals were gently washed with water over a Büchner-type filtration system and then dried under N_2 in order to remove the adventitious surface oxidation products. Then, a prescribed amount of the previously washed sodium sulfide was added to the buffer solution (300 mL) turning virtually all the sulfide ions into bisulfide anions at the prevailing pH conditions. A 5-mL aqueous suspension of the iron-containing material was abruptly injected in the reactor to trigger reaction. During the course of reaction, small aliquots (1 mL) were periodically withdrawn from the reactor and filtered on a Millipore membrane filter to remove solid particles larger than 0.2 μm. The samples were split in two parts: one part (0.7 mL) was analyzed by capillary electrophoresis (CE) to monitor the evolution of residual bisulfide and the formed sulfur-bearing products; a second part (0.3 mL) was diluted in 25 mL of water and then analyzed by atomic absorption spectroscopy to quantify dissolved iron. The samples containing the sulfur-bearing products were kept in glove-box-like equipment under oxygen-free atmosphere (nitrogen) prior to CE analysis.

Polysulfide synthesis

The polysulfides were synthesized using a method detailed elsewere.[30] The polysulfides solution was prepared in 50 mL sealed glass flasks by dissolving 0.45 g of sodium sulfide nonahydrate and 0.061 g of elemental sulfur (1:1 S-to-HS^- mole ratio) in the corresponding buffer (pH = 9.5) which was subsequently oven-heated at 65°C during 4 h. To observe the influence of the concentrations ratio of initial bisulfide and zerovalent sulfur, solutions with two initial mole ratios S:HS^-(1:1, 5:1) were prepared. After synthesis, each polysulfides solution contained, aside from polysulfides, a mixture of unreacted bisulfide and solid sulfur. The solutions were therefore filtered through 11 μm membrane pore filters (Micropore) to eliminate residual undissolved solid sulfur prior to reaction. For the reactions with Fe/Ce oxide–hydroxide, 50 mL of concentrated polysulfides solution were

diluted with the buffer to a final volume of 300 mL and the reaction was initiated as described in the previous section.

Sample analysis

Bisulfide consumption and possible products (thiosulfate, sulfate, sulfite, and polysulfides) formation were monitored by means of a capillary electrophoresis (CE) system (Agilent Technologies) used to separate, identify, and quantify the ionic species being formed or consumed during the reaction. The CE prootocle was thoroughly detailed elsewere.[29,30] The dissolved iron was analyzed as a Fe-polydentate complex by means of an atomic absorption spectrometer (Perkin-Elmer), as detailed elsewere.[29] The polydentate complex used was the 1,3-diaminopropane-*N,N,N′,N′*-tetraacetic acid (PDTA), purchased from Sigma-Aldrich Canada. The experimental error was about 1 mg/L for the CE analysis and 1 μg/L for the atomic absorption spectrometer analysis.

Results

Iron dissolution and sulfur speciation

To prevent precipitation of the ferrous cations after dissolution, a small quantity of a polydentate chelating agent was added to the borate buffer prior to reaction. To serve the analytical purposes of this study, the ligand used must meet two conditions: (i) it must rapidly form a ferrous complex that remains stable enough during the analysis time; (ii) the ferrous-ligand complex must exhibit very poor reactivity towards adventitious dissolved oxygen that might have involuntarily gotten in during sample manipulations. One example of ligands meeting both requirements was found to be PDTA,[29] which was used here to quantify the concentration of dissolved Fe^{2+}.

At this stage, an obvious distinction must be made also between the moles of divalent iron that form on the material's surface according to stoichiometry and the moles of divalent iron that leach off from the material's surface and which are indeed those concerned with detection and quantification. The latter will be referred to "leached Fe^{2+}". Hence, the quantity of leached iron thus measured cannot be used as a measure of the transferred electrons between sulfur and oxide-hydroxide.

A 90% removal level of HS^- was reported at pH = 9.5 after 180 min of reaction, whereas the corresponding Fe^{2+} that leached off represented on a molar basis only ~15% of converted bisulfide.[29] Thiosulfate was found to be the major oxysulfur product that built up in the solution, whereas polysulfides, while accumulating over the first 90 min of reaction, started to decline afterwards.[29] While sulfite and tetrathionate remained below instrumental detection limits (<1 ppm), only marginal amounts of sulfate accumulated over a reaction time span of 180 min suggesting that disproportionation of thiosulfate into sulfate and bisulfide is, as expected,[31] not favorable at 25°C. Mechanistic interpretations on the formation via a heterogeneous pathway of thiosulfate at the expense of sulfate will be discussed in more detail in the forthcoming Discussion section. Pyzic and Sommer[22] also found elemental sulfur (ca. 85%) present as zerovalent sulfur and polysulfides, and thiosulfate (ca. 15%) to be the major products of bisulfide oxidation by goethite at pH = 8. According to Petre and Larachi,[29] the produced thiosulfate represented 16% of the consumed bisulfide after 180 min. It was suggested in accordance with the CE identified sulfur species that the zerovalent sulfur products (polysulfides and elemental sulfur) must have represented the rest of about 84% of the bisulfide converted at pH = 9.5 in line with previous findings.[22] Petre and Larachi[29] also found that the molar ratio of leached iron (i.e., PDTA chelated Fe^{2+}) to the produced thiosulfate neared unity at pH = 9.5 suggesting a direct correlation between the formation mechanisms of the two products.

Figures 1a,b show that the bisulfide oxidation and iron dissolution rates are decreasing with increasingly pH coherent with literature findings.[23–26] For HS^- (Figure 1a), at pH = 8 the conversion was total before 40 min, while at pH = 11, the conversion was less than 55% after 180 min. The dissolved Fe^{2+} at pH = 8 (Figure 1b) corresponded to >60% (molar basis) of converted bisulfide after 180 min, while at pH = 11 and after the same time period, this proportion fell

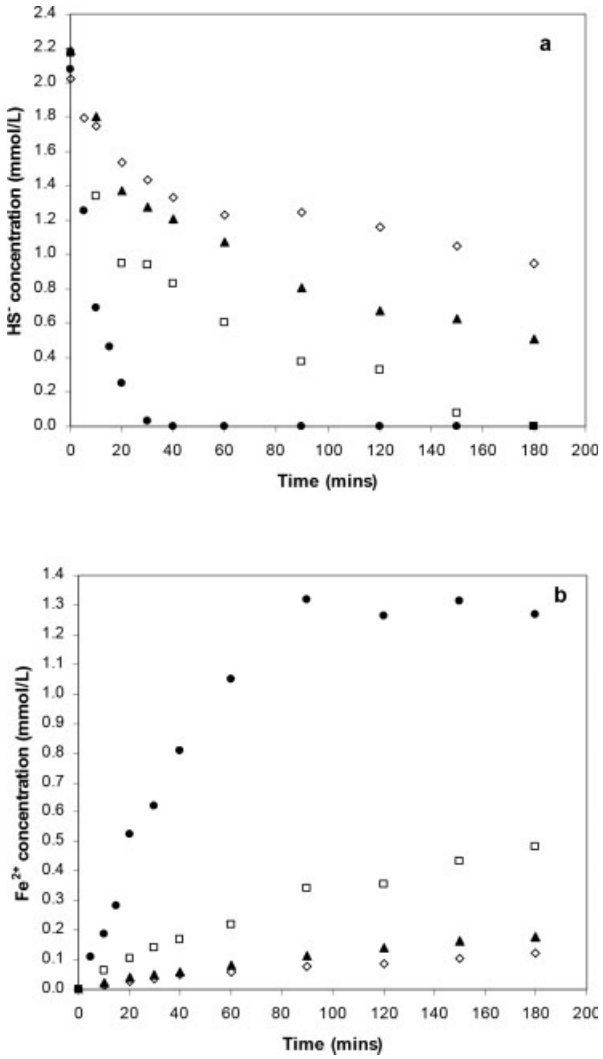

Figure 1. pH-induced bisulfide oxidation (a) and leached iron production (b) for the reaction between the Fe/Ce oxide–hydroxide and bisulfide (in 100 mmol/L borate + 0.5 mmol/L PDTA, 25°C, 1 atm): (●) pH = 8, (□) pH = 9, (▲) pH = 10, and (◇) pH = 11.

below 17% of oxidized bisulfide. The molar ratio of thiosulfate to leached iron was found to be equal to one inasmuch as the pH exceeded 9. At lower pH values, however, this ratio dropped considerably (data not shown). This suggests that the role of pH in the reaction between HS^- and Fe/CeOx is double. While decreasing pH obviously enhances bisulfide oxidation by surface iron (Figure 1a), lower pH also promotes the extent of iron leaching (Figure 1b) suggesting different reaction paths for iron leaching as a function of pH.

Influence of reaction products on bisulfide oxidation and iron dissolution

Polysulfides are known to be key intermediates in the bisulfide oxidation by both dioxygen[32,33] and ferric iron[29,33] at neutral-to-alkaline pH. To assess in what extent polysulfides can influence the bisulfide oxidation kinetics, two polysulfides solutions with different concentrations were prepared and then tested in the reaction with Fe/CeOx.

The results with the first solution (5:1 initial mole ratio elemental sulfur-to-bisulfide) are compared in Figures 2a,b with those of a solution initially containing bisulfide only but at nearly equal bisulfide concentrations (ca. 1.5 mmol/L HS^-). The presence of a significant concentration of nonnascent polysulfides barely affected the time evolution of iron leaching and thiosulfate production. On the contrary, the presence of nonincipient polysulfides appears to delay the bisulfide consumption, especially after the initial stage around 40 min (Figure 2a). The 1:1 mole ratio between dissolved iron and produced thiosulfate, as observed previously (Figure 1a), persists also in the case of pre-existing polysulfides (Figures 2a,b). This observation suggests that iron leaching and thiosulfate formation depend only on bisulfide and Fe/Ce oxide–hydroxide initial concentrations and are not related to the presence, and especially the accumulation, of polysulfides in the course of bisulfide conversion.

Figures 3a,b compare the evolution of bisulfide, leached iron (Figure 3a) and thiosulfate (Figure 3b) for the second solution of polysulfides (1:1 initial mole ratio elemental sulfur-to-bisulfide) along with its companion bisulfide-only solution. For initially nearly equal bisulfide concentrations with and without nascent polysulfides (ca. 2.7 mmol/L HS^-), more bisulfide was left unconverted ultimately in the 1:1 S-HS^- solution (Figure 3a). This suggests, as in Figure 2a, that direct interactions occurred between the polysulfides and the Fe/Ce oxide-hydroxide sites thus hindering the approach and access of bisulfide to the iron sites. Because polysulfides are stronger nucleophiles than bisulfide,[33] their reaction with the active ferric surface sites is likely to be fast with, thus, direct repercussions on the bisulfide consumption (Figures 2a and 3a). Here again, the presence of pre-existing polysulfides along with bisulfide had no influence on iron dissolution or on thiosulfate formation (Figures 3a,b).

Figures 4a,b show the influence of foreign sulfite on the reaction kinetics between bisulfide and Fe/Ce oxide–hydroxide. The presence of sulfite at the beginning of the reaction appears to have a beneficial influence on bisulfide consumption, whereas Fe^{2+} appears to be less prone to leaching (Figure 4a). This can be explained according to the following reaction[31]:

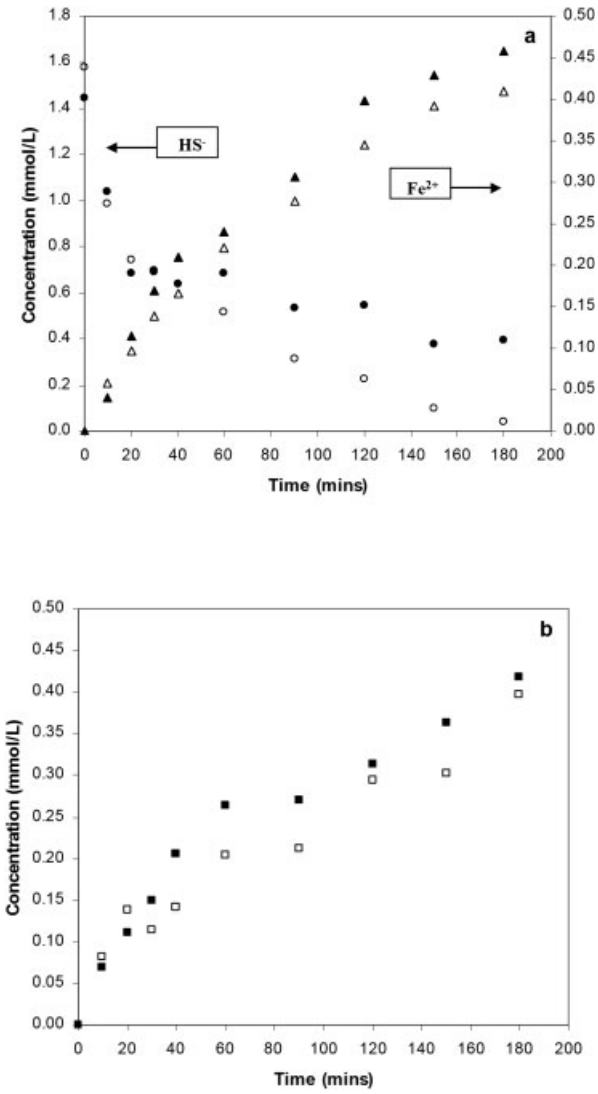

Figure 2. Effect of polysulfides (initial ratio S-to-HS 5:1) on bisulfide consumption and iron dissolution (in 100 mmol/L borate + 0.5 mmol/L PDTA, 25°C, 1 atm, pH = 9.5): (a) HS^- + S_x^{2-} solution [(●) bisulfide oxidation and (▲) iron dissolution] compared with HS^- solution [(○) bisulfide oxidation and (△) iron dissolution]; (b) evolution of thiosulfate for (■) HS^- + S_x^{2-} solution and (□) HS^- solution.

$$S_nS^{2-} + nSO_3^{2-} + H_2O \rightarrow nS_2O_3^{2-} + HS^- + OH^- \qquad (R8)$$

which will likely accelerate the consumption of (longer-chain) polysulfides. In return, perturbation of the mutual equilibria between the different polysulfides would accelerate the consumption of bisulfide despite one bisulfide is released back by (R8) for each converted polysulfide. An intuitive argument in favor of this behavior is as follows: according to reaction (R8), one mole bisulfide is produced when one mole *n*-polysulfides are consumed. For illustration purposes assuming that polysulfides equilibria would attempt to recover back

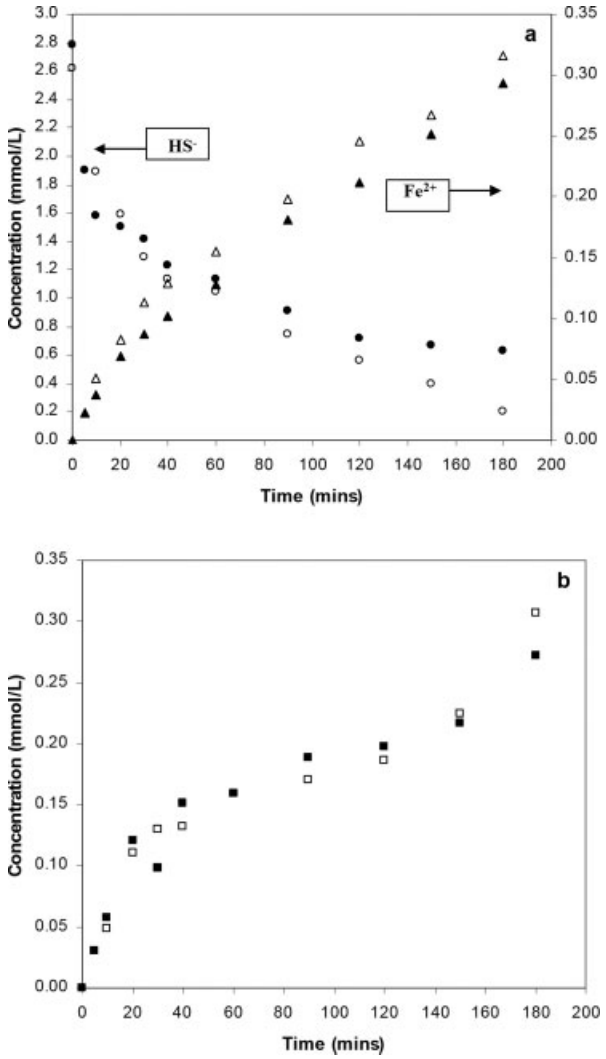

Figure 3. Effect of polysulfides (initial ratio S-to-HS 1:1) on bisulfide consumption and iron dissolution (in 100 mmol/L borate + 0.5 mmol/L PDTA, 25°C, 1 atm, pH = 9.5): (a) HS^- + S_x^{2-} solution [(●) bisulfide oxidation and (▲) iron dissolution] compared with HS^- solution [(○) bisulfide oxidation and (△) iron dissolution]; (b) evolution of thiosulfate for (■) HS^- + S_x^{2-} solution and (□) HS^- solution.

the consumed *n*-polysulfides mole, oxidation of n more moles bisulfide would be necessary to counteract the disturbance of polysulfides by R8. Hence *n*-1 extra moles of bisulfide would be needed to restore the same polysulfides concentration with qualitatively a net result of more bisulfide consumption as illustrated in Figure 4a. On the other hand, and as will be explained later, the slowdown of released dissolved Fe^{2+} could result from diversion of the disulfide–iron–thiosulfate route towards a disulfide–polysulfide route.

In Figure 4b, the cumulative thiosulfate produced over 180 min is contributed by the sulfite-mediated thiosulfate via (R8) along with that generated from the reaction between bisulfide and Fe/Ce oxide–hydroxide (Figures 1–3). Virtually no sulfate was produced over the time duration of our experiments (Figure 4b). Once again, the results shown in Figures 4a,b indicate that the leaching of iron and the formation of thiosulfate are interrelated and plausibly adhere to the same formation mechanism yielding the 1:1 mole ratio observed above at pH = 9.5.

The reaction between bisulfide and Fe/Ce oxide–hydroxide exhibits virtually no sensitivity to the presence of pre-existing thiosulfate (0.5 mmol/L) introduced in the aqueous medium before reaction is triggered (Figure 5). Both bisulfide oxidation and ferrous iron dissolution profiles are very close

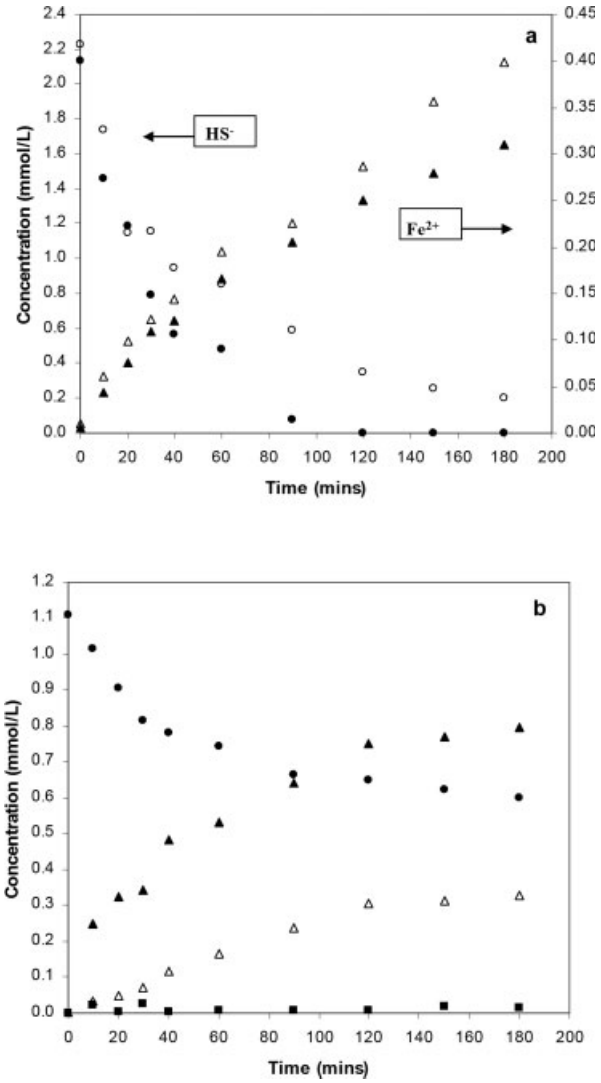

Figure 4. Effect of sulfite on bisulfide consumption and iron dissolution (in 100 mmol/L borate + 0.5 mmol/L PDTA, 25°C, 1 atm, pH = 9.5); (a) SO_3^{2-} + HS^- solution [(●) bisulfide oxidation and (▲) iron dissolution] compared with HS^- solution [(○) bisulfide oxidation and (△) iron dissolution]; (b) evolution of oxidation products: SO_3^{2-} + HS^- solution [(●) sulfite, (▲) thiosulfate and (■) sulfate] compared with HS^- solution [(△) thiosulfate].

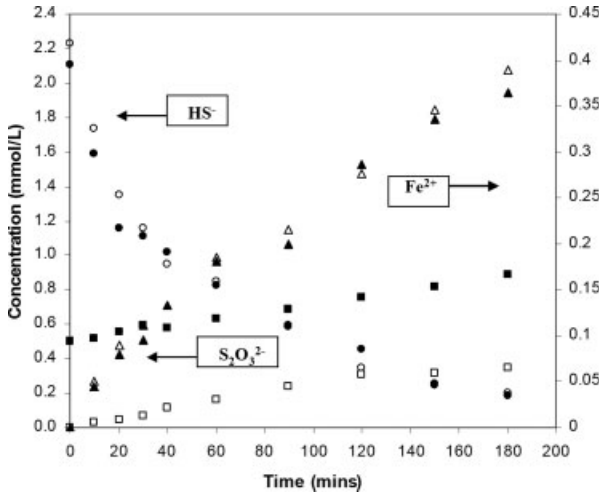

Figure 5. Effect of thiosulfate on bisulfide consumption and iron dissolution (in 100 mmol/L borate + 0.5 mmol/L PDTA, 25°C, 1 atm, pH = 9.5): $S_2O_3^{2-}$ + HS^- solution [(●) bisulfide oxidation, (■) thiosulfate and (▲) iron dissolution] compared with HS^- solution [(○) bisulfide oxidation, (□) thiosulfate and (△) iron dissolution).

to the ones obtained in runs experiencing only the buildup of incipient thiosulfate. Note that the $S_2O_3^{2-}$ produced in the two reaction tests follows the same profiles except the offset corresponding to the initial thiosulfate concentration of the $S_2O_3^{2-}$ + HS^- solution. Furthermore, when thiosulfate was substituted with an equal amount of sulfate added at the beginning of the reaction, the bisulfide consumption and both Fe^{2+} and $S_2O_3^{2-}$ productions remained unaltered with respect to the base case of bisulfide-only solution.

Figure 6 mirrors the time evolution of the Fe/Ce oxide–hydroxide BET specific surface area with that of bisulfide residual concentration. It was shown previously[29] that the reaction between HS^- and Fe/Ce oxide–hydroxide is a two-step surface-controlled reaction. The first step, relatively rapid, confines to the early about 30 min and contributes to eliminate 50% of bisulfide (see Figures 2a, 3a, and 4a). The subsequent step evolves at a slower HS^- oxidation rate. This difference in paces could be ascribed to different types of Fe(III) surface sites being accessed by HS^- during the reaction course. While in the first step, the reaction rate is controlled by the bisulfide-promoted reduction of the most accessible Fe(III) surface sites, in the second step the reaction rate becomes controlled likely by less accessible Fe(III) reaction sites and also by the rate of dissolution of Fe(II). These interpretations seem to be supported by the similar shapes (and equal slopes) exhibited by the BET surface area and the bisulfide residual concentration curves versus time (Figure 6). The surface area dropped by 12% within the early 30 min, which was followed by a further 9% loss in the second step (30–180 min).

Analysis of the BJH desorption average pore diameter indicated that the pore size kept virtually unaffected during reaction between Fe/CeOx and bisulfide. On the contrary, the evolution of BJH desorption cumulative pore volumes decreased with time as for the surface area (Figure 6). For constant pore diameter, decreasing the cumulative pore volume (and consequently surface area) with reaction time suggests that after interacting with bisulfide, some of the Fe/Ce oxide–hydroxide pores vanish. In our opinion, this behavior can be ascribed to particles detachment during reaction combined to blocking of small pores with reaction products, e.g., elemental sulfur or polysulfides.

XPS studies

The Fe/Ce oxide–hydroxide samples of three representative experiments were analyzed by XPS (Figures 7–10). Prior to XPS analysis, the powder samples were recovered by filtration after reaction, washed with de-ionized water, and then dried at 120°C for 3 h under nitrogen atmosphere.

The inorganic sulfur has four known (stable) oxidation states: S(−II), S(0), S(+IV) and S(+VI). To identify the signature of each of the two sulfur atoms present in thiosulfate, $Na_2S_2O_3$ powdered salt was analyzed. The results presented in Table 1 (lines 33,34), in agreement with the literature,[51] showed two distinct signatures relevant to two oxidation states. The first sulfur, bonds solely to the second sulfur, is assigned to S(−II) (Table 1, lines 16,33), while the second sulfur bonds also to three oxygen atoms and is characterized by a higher BE value at 167.30 eV which is assigned to S(+VI) (Table 1, lines 30,32,34). Samples of solid sulfur were also analyzed to establish the signature of zerovalent sulfur, S(0). The results of the analysis of the S 2p core level spectra were in agreement with the literature[24,29–31,42,45–47] and showed one photoelectron peak at 163.8 eV (Table 1, line 28).

Figures 7a,b show, respectively, the XP core level spectra of sulfur (S 2p) and oxygen (O 1s) for a usual Fe/CeOx sample recovered after reaction with bisulfide (s no. 1). The S 2p

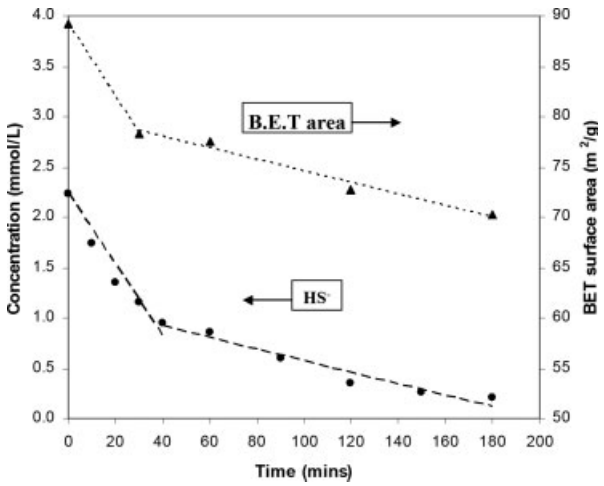

Figure 6. Comparison between the Fe/Ce oxide–hydroxide evolution of the BET specific surface area and the bisulfide consumption profiles (in 100 mmol/L borate + 0.5 mmol/L PDTA, 25°C, 1 atm, pH = 9.5, initial surface area = 89.2 m^2/L).

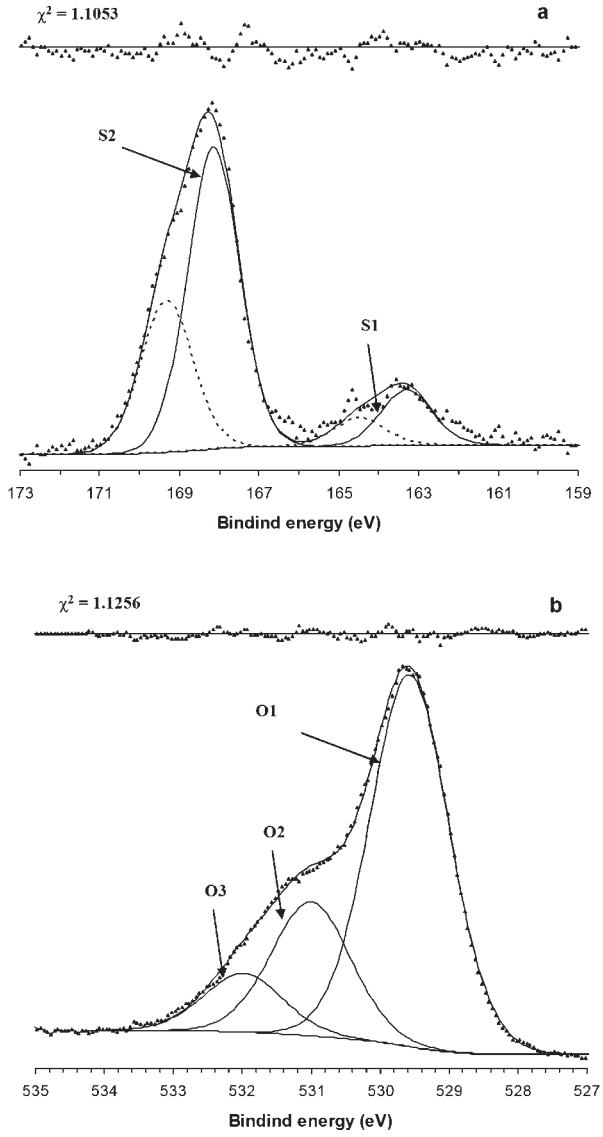

Figure 7. Fe/Ce oxide–hydroxide XP spectra of (a) S 2p and (b) O 1s, after 180 min of reaction with bisulfide (s no. 1).

Solid and dotted lines are representing the S 2p2/3 and, respectively, S 2p1/2 components of the S 2p spectra. Experimental conditions: 100 mmol/L borate + 0.5 mmol/L PDTA at pH = 9.5, 25°C, 1 atm, Fe/CeOx initial surface area = 109.8 m^2/L, HS^-_{ini} = 2.04 mmol/L.

spectrum reveals the presence of two sulfur species. The first (S1 in Figure 7a), with BE = 163.3 eV for S 2p3/2 contributes about 15% of the total sulfur and can be attributed to a combination of S(0) and S(−II) corresponding most likely to polysulfides, S_n^{2-} (Table 1, line 26). The second sulfur species (S2 in Figure 7a), with BE = 168.2 eV for S 2p3/2 was overwhelming (ca. 85%) and can be attributed to the highest oxidation state sulfur S (+VI) present in both sulfate (Table 1, line 30) and thiosulfate (Table 1, line 32).

The O 1s peak was decomposed (Figure 7b) into three components at 529.6, 531.0, and 532.0 eV associated, respectively, with oxygen from oxides, hydroxides, and molecular water (Table 1, lines 35–39). The first component (O1 in Figure 7b), attributed to oxygen from oxides, was the most abundant (ca. 65%) and stems, most probably, from a combination of signatures for iron (29%), carbon (10%), cerium (2.9%), sulfur (2.7%), and boron (1.4%) oxides. The second component (O2 in Figure 7b) of the O 1s spectra contributed for about 24% and is ascribed most probably to hydroxyl groups from the Fe hydroxide (Table 1, line 37), while the last component (O3 in Figure 7b) is likely due to the presence of molecular water adsorbed at the sample surface (Table 1, line 39).

The effect of non-nascent polysulfides in the reaction between the Fe/Ce oxide–hydroxide and bisulfide (s no. 2) is shown in terms of XP spectra of both sulfur (S 2p) and oxygen (O 1s) in Figure 8. The solution of polysulfides was prepared as in Figure 2 (5:1 initial mole ratio elemental sulfur-to-bisulfide). The S 2p core level spectrum is far more complex in comparison to that of Figure 7a and where at least four components could be identified (Figure 8). The first (S1, Figure 8) at BE = 161.9 eV of the S 2p3/2 represents about 10% of the total sulfur and was assigned to S(-II) (Table 1, line 16). The second (S2, Figure 8) and most important component (ca. 43%) is positioned at BE = 163.4 eV and can be attributed to zerovalent sulfur (Table 1, line 16) or to polysulfides-type sulfur (Table 1, line 16). The dominance of the S 2p3/2 component at 163.4 eV is logically explained by the presence of large quantities of polysulfides in the reaction medium. The polysulfides react with Fe/Ce oxide–hydroxide to form colloidal sulfur, which is another source of zerovalent sulfur, corroborating the magnitude of the 163.4 eV peak. The third component (S3, Figure 8) in the sulfur spectrum lying at 166.8 eV can be attributed to S(+IV) from a

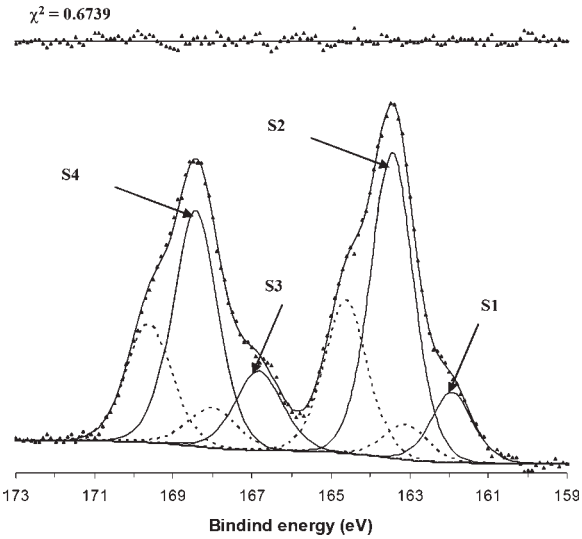

Figure 8. Fe/Ce oxide–hydroxide XP spectra of S 2p, after 240 minutes of reaction with a mixture bisulfide-polysulfides (s no. 2).

Solid and dotted lines are representing the S 2p2/3 and, respectively, S 2p1/2 components of the S 2p spectra. Experimental conditions: 100 mmol/L borate + 0.5 mmol/L PDTA at pH = 9.5, 25°C, 1 atm, Fe/CeOx initial surface area = 112.2 m^2/L.

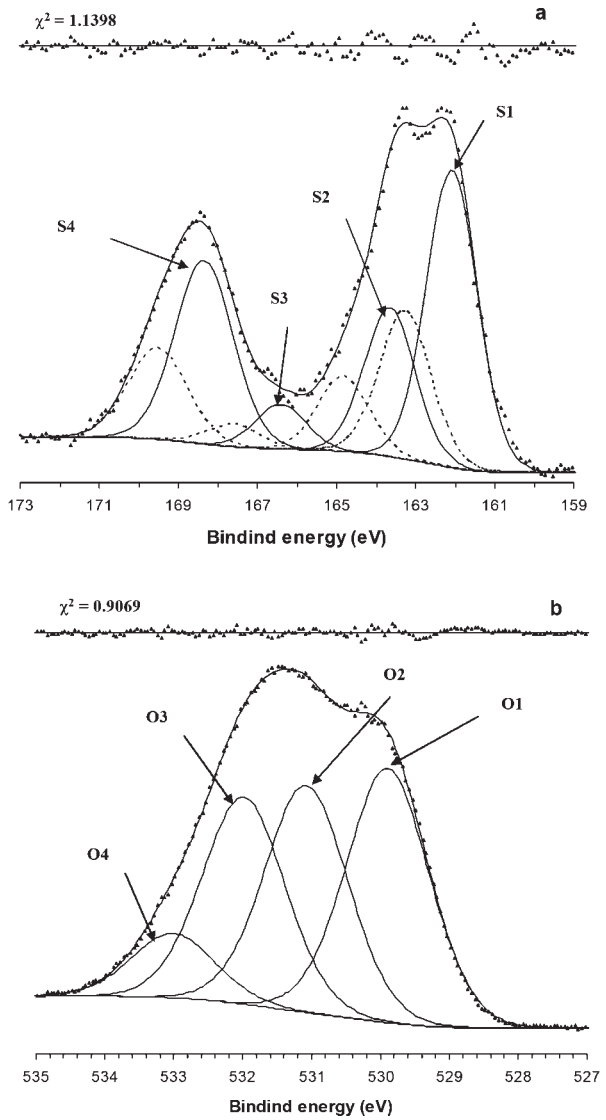

Figure 9. Fe/Ce oxide–hydroxide XP spectra of (a) S 2p and (b) O 1s, after 48 h of reaction with excess bisulfide (s no. 3).

Solid and dotted lines represent, respectively, S 2p2/3 and S 2p1/2 components of S 2p spectra. Experimental conditions: 100 mmol/L borate at pH = 9.5, 25°C, 1 atm, Fe/CeOx initial surface area = 112.0 m^2/L, HS^-_{ini} = 20.16 mmol/L.

sulfite-type structure (Table 1, line 29), while the last signature (S4, Figure 8a, ca. 35% at 168.4 eV) is due, as explained earlier, to the presence of S(+VI) from sulfate and/or thiosulfate-type structures (Table 1, lines 30-34).

Analysis of the O1s core level spectra for the material taken from the reaction between the polysulfides–bisulfide mixture and Fe/CeOx (s no. 2) enabled identification, as in the case of Figure 7b, of three components: O^{2-} of oxides at 529.9 eV; hydroxyl groups at 531.3 eV and water at 532.2 eV (Table 1, lines 35-39). These components appeared to be in correspondingly comparable proportions with those of Figure 7b, with the oxygen from oxides having the most important contribution (ca. 65%).

S 2p and O 1s XP core level spectra for the Fe/CeOx sample (s no. 3) isolated after 48 h of reaction with excess bisulfide (20 mmol/L) are shown in Figures 9a,b. The reaction test corresponding to this analysis had two main goals. The first was to detect the formation of iron monosulfide precipitate via reaction (R7); while the second was to enable accumulation of enough colloidal sulfur from the polysulfides oxidation to validate its XPS detection. The overwhelming signature at BE = 162.1 eV of the S 2p3/2 peak (S1, Figure 9a) representing a sulfur species about 42% in abundance can be attributed, most probably, to the formation of iron sulfide species, FeS_x (Table 1, lines 19, 20). The second component (S2, Figure 9a), whose peak is located at 163.7 eV, designates the signature of zerovalent sulfur from colloidal sulfur and/or polysulfides (Table 1, lines 22,27). The quantity of zerovalent sulfur produced is meaningfully greater for s no. 3 than s no. 1. The remaining two components of the S 2p spectra (S3 and S4, Figure 9a) correspond to sulfoxy species: SO_3^{2-}-like structure at 166.4 eV and SO_4^{2-} and /or $S_2O_3^{2-}$-like structures at 168.4 eV.

The XP O 1s spectrum recorded for the Fe/Ce oxide–hydroxide isolated after 48 h reaction with excess bisulfide (s no. 3) is shown in Figure 9b. Spectral decomposition resulted in four oxygen-containing species with BE located at 529.9 eV (O1), 531.1 eV (O2), 531.9 eV (O3) and 533.1 eV (O4). Besides the three peak assignments identified earlier (Table 1, lines 35-39), a fourth oxygen peak was required to

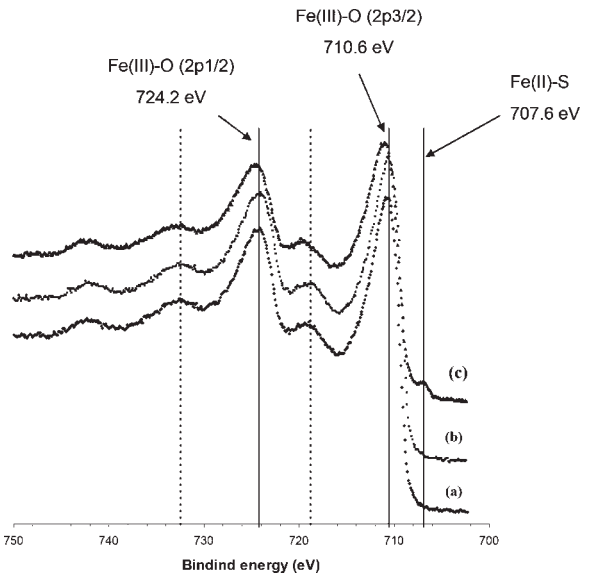

Figure 10. Comparison between XP spectra of Fe 2p for (a) reaction between Fe/Ce oxide–hydroxide and HS^- (s no. 1, conditions as in Figure 7), (b) reaction between Fe/Ce oxide–hydroxide and a mixture HS^- and S_x^{2-} (s no. 2, conditions as in Figure 8) and (c) reaction between Fe/Ce oxide–hydroxide and excess HS^- (s no. 3, conditions as in Figure 9).

Solid lines represent positions for main photoelectron peaks, while dotted lines represent positions for charge transfer satellites.

improve the fit. Because of many fitting possibilities, its physical assignment remains unclear and was not attempted in the present study.

Figure 10 compares the Fe 2p XP spectra corresponding to the spent Fe/CeOx s no. 1, s no. 2, s no. 3 samples discussed above (Figures 7–9). The Fe 2p photoelectron spectra are characterized by the presence of two main components, Fe 2p3/2 and Fe 2p1/2, each associated with a charge transfer satellite peak.[48] Depending on the oxidation state and nature of the chemical species bonding to iron, the Fe 2p3/2 and Fe 2p1/2 photoelectron peaks occupy different BE positions (Table 1, lines 1–15). Hence, for the first two samples s no. 1 and s no. 2, respectively, curves (a) and (b) (Figure 10), the corresponding Fe 2p3/2 peak is located at 710.6 eV with its companion satellite at 718.7 eV. Correspondingly, the Fe 2p1/2 is located at 724.2 eV and its satellite at 732.4 eV. The combined information from Table 1 (lines 14,15) and Figure 10 curves (a) and (b) suggests that iron present at the surface of both samples s no. 1 and s no. 2 is made up of a mixture of Fe(III) oxides and hydroxides.

The Fe 2p XP spectrum of sample s no. 3 (curve (c), Figure 10) exhibits some dissimilarity with regard to s no. 1 and s no. 2 samples. The first, and probably most important, difference arises from the small peak at 707.0 eV which confirms the existence of a FeS_x structure on the sample surface (Table 1, line 6). The formation of FeS_x subsequently to iron hydroxide leaching by bisulfide has been reported in previous laboratory studies and could contribute to the total dissolved Fe pool at pH $\geq$ 7.[25] Moreover, pyrite (FeS_2) was shown to be the thermodynamically stable end-product of the reaction between iron hydroxides with sulfide produced from sulfate reduction in marine sediments.[64] Therefore, the reaction between Fe/CeOx and bisulfide can yield to the formation of iron sulfide as suggested by the 707 eV peak in Figure 10 [curve (c)]. The second difference observed from Figure 10 between curves (a)–(c) is the Fe 2p3/2 peak shift from 710.6 [curves (a) and (b)] to 711.0 eV [curve (c)]. The Fe 2p3/2 peak at 711.0 eV is specific to a Fe(II) linked to sulfate as reported by Decostes et al.[48] This observation leads us to conclude that s no. 3 sample surface contains, besides a mixture of Fe(III) oxides and hydroxides and Fe(II) sulfide traces, some Fe(II) connected to sulfoxy species such as $Fe—S_2O_3$ or/and $Fe—SO_4$.

Discussion

Formation mechanism of polysulfides, elemental sulfur, thiosulfate, and leached iron

Laboratory kinetic data on the anoxic chemical oxidation of bisulfide by Fe(III) oxides-hydroxides revealed, besides the zerovalent sulfur products, such as polysulfides[19,22] and elemental sulfur,[19,21–26] the formation of sulfoxy compounds including thiosulfate[19,21,22] and sulfate.[23–27] Despite all the available kinetic data, no satisfactory mechanism clearly depicts the electron transfer processes at the oxide surface between the reducing agent, i.e., HS^-, and the oxidant species, i.e., Fe(III), to explain the formation of all above-mentioned detected products. Basolo and Pearson[65] showed that electron transfer processes between metal surface sites and adsorbed surface species are limited to only one or two electrons at a time. On the basis of these observations, Hering and Stumm[66] elegantly described an inner-sphere electron transfer process between two metals bound through a common (bridging) ligand. The oxidation of pyrite by iron hydroxides using electron transfer processes in which an electron from the SS^{2-} in pyrite is transferred to Fe(III) was explained by Luther III[67] from the oxide surface by means of an inner sphere type mechanism and molecular orbital theory. The first electron transfer in oxidation of pyrite occurs from the π^* orbital (highest occupied molecular orbital) of the S_2^{2-} in FeS_2 to the π orbital (lowest unoccupied molecular orbital) of the oxidant, i.e., iron hydroxide.[67] The bridge mechanism involving two metal entities via a common ligand (persulfido) followed by electron transfer was consistent with an inner-sphere type mechanism. In another study, Moses et al.[68] suggested that additional bridges could be formed on the FeS_2 surface during oxidation until the final oxidation product, $S_2O_3^{2-}$, is produced. These authors[67,68] concluded that the proposed mechanism does not require the formation of a free radical in solution but speculated the formation of an ion radical on the pyrite surface. They also explained that the strength of the sulfur–sulfur bond in the persulfido bridge after electron transfer is key to the understanding of FeS_2 oxidation.

Based on the above considerations and on experimental observations, the anoxic alkaline oxidation of bisulfide by Fe and/or Fe/Ce oxides–hydroxides is proposed to proceed via the reaction pathway summarized in Table 2. The reaction pathway elaborated for pH $\geq$ 8 shows the formation steps of zerovalent (polysulfides and elemental sulfur), sulfoxy (thiosulfate) and Fe^{2+} species. The detailed pathway is broken down into three main parts. The first part rationalizes the formation of disulfide (SS^{2-}) which is believed to be the first and key sulfur-intermediate product in bisulfide oxidation (Table 2, part A). As explained by Steudel,[31,33] the oxidation of bisulfide by ferric ion, oxygen or other oxidants proceeds via a radical mechanism with the formation of disulfide, the smallest polysulfide oligomer. The formation of disulfide is believed to be controlled by the formation of sulfide radical, $S^{-\bullet}$.[31,33] In the case of HS^- oxidation by Fe(III) hydroxide, the formation of sulfide radical is very fast and proceeds in three steps as proposed by dos Santos Afonso and Stumm.[23] The three steps depicted in part A of Table 2 are: (i) bisulfide adsorption at the oxide surface, (R1); (ii) electron transfer between Fe(III) site and S^{2-}, (R2); (iii) release of $S^{-\bullet}$ and formation of surface-protonated site [$Fe^{II}(OH_2)^+$], (R3). On the basis of the previous observations,[67,68] it is proposed here that the sulfur radical will not leave the inner-sphere layer giving the opportunity for the formation of a disulfide according to (R9).

Steudel[31,33] showed that disulfide is even a stronger reducing agent then bisulfide. Therefore it will react with another Fe(III) site to form an iron-disulfide surface complex: Table 2 part B, reactions (R10), (R11) for $n = 2$ and Table 2 part C, reactions (R17), (R18). The proposed pathway makes the presumption that disulfide will not leave the inner-sphere layer and, consequently, the reaction with the iron site will be very fast. The [$Fe^{II}(SS)$] surface complex is stoichiometrically identical with pyrite but has a different structure and therefore different chemical properties. The (SS^-) ligand in the above-mentioned complex structure is unique. Its formal charge is (−I), with one S(0) and a second sulfur bonded to Fe(II) having a (−I) charge. This second sulfur had initially

Table 2. Polysulfides, Elemental Sulfur, Thiosulfate, and Divalent Iron Formation Steps* from Bisulfide Oxidation by Fe/Ce Oxide–Hydroxide for pH $\geq$ 8

A. Formation of disulfide steps

$$[Fe^{III}(OH)] + (HS^-) \underset{k_{g-1}}{\overset{k_{g1}}{\rightleftarrows}} [Fe^{III}(S)^-] + H_2O \quad (R1)$$

$$[Fe^{III}(S)^-] \underset{k_{g-2}}{\overset{k_{g2}}{\rightleftarrows}} [Fe^{II}(S)] \quad (R2)$$

$$[Fe^{II}(S)] + (H_2O) \underset{k_{g-3}}{\overset{k_{g3}}{\rightleftarrows}} [Fe^{II}(OH_2)^+] + (S^{-\bullet}) \quad (R3)$$

$$2(S^{-\bullet}) \underset{k_{g-4}}{\overset{k_{g4}}{\rightleftarrows}} (SS^{2-}) \quad (R9)$$

B. Formation of polysulfides and elemental sulfur steps

(I) Formation of iron–polysulfide surface complex (n = 2–8)

$$[Fe^{III}(OH)] + (S_{n-1}S^{2-}) \underset{k_{s-1n}}{\overset{k_{s1n}}{\rightleftarrows}} [Fe^{III}(S_{n-1}S)^-] + (OH^-) \quad (R10)$$

$$[Fe^{III}(S_{n-1}S)^-] \underset{k_{s-2n}}{\overset{k_{s2n}}{\rightleftarrows}} [Fe^{II}(S_{n-1}S)] \quad (R11)$$

(II) Polysulfides chain growth (n = 2–8)

$$[Fe^{II}(S_{n-1}S)] + (HS^-) \underset{k_{s-3n}}{\overset{k_{s3n}}{\rightleftarrows}} [Fe^{II}(S_nS)^{2-}] + (H^+) \quad (R12)$$

$$[Fe^{II}(S_nS)^{2-}] + [Fe^{III}(OH)] \underset{k_{s-4n}}{\overset{k_{s4n}}{\rightleftarrows}} [Fe^{II}(S_nS)^{2-} \mapsto Fe^{III}(OH)] \quad (R13)$$

$$[Fe^{II}(S_nS)^{2-} \mapsto Fe^{III}(OH)] \underset{k_{s-5n}}{\overset{k_{s5n}}{\rightleftarrows}} [Fe^{II}(S_nS)^- \mapsto Fe^{II}(OH)] \quad (R14)$$

$$[Fe^{II}(S_nS)^- \mapsto Fe^{II}(OH)] + 2(H_2O) \underset{k_{s-6n}}{\overset{k_{s6n}}{\rightleftarrows}} S_nS^{2-} + 2[Fe^{II}(OH_2)^+] + OH^- \quad (R15)$$

(III) Formation of elemental sulfur

$$S_8S^{2-} + H^+ \underset{k_{s-7}}{\overset{k_{s7}}{\rightleftarrows}} S_8 + HS^- \quad (R16)$$

C. Formation of thiosulfate steps

(I) Formation of surface iron–disulfide complex

$$[Fe^{III}(OH)] + (SS^{2-}) \underset{k_{t-1}}{\overset{k_{t1}}{\rightleftarrows}} [Fe^{III}(SS)^-] + (OH^-) \quad (R17)$$

$$[Fe^{III}(SS)^-] \underset{k_{t-2}}{\overset{k_{t2}}{\rightleftarrows}} [Fe^{II}(SS)] \quad (R18)$$

(II) Formation of first sulfur–oxygen surface intermediate

$$[Fe^{II}(SS)] + [Fe^{III}(OH)] \underset{k_{t-3}}{\overset{k_{t3}}{\rightleftarrows}} [Fe^{II}(SS) \mapsto Fe^{III}(OH)] \quad (R19)$$

$$[Fe^{II}(SS) \mapsto Fe^{III}(OH)] \underset{k_{t-4}}{\overset{k_{t4}}{\rightleftarrows}} [Fe^{II}(SS)^+ \mapsto Fe^{II}(OH)] \quad (R20)$$

$$[Fe^{II}(SS)^+ \mapsto Fe^{II}(OH)] + (H_2O) \underset{k_{t-5}}{\overset{k_{t5}}{\rightleftarrows}} [Fe^{II}(SS{-}OH)] + [Fe^{II}(OH_2)^+] \quad (R21)$$

$$[Fe^{II}(SS{-}OH)] + [Fe^{III}(OH)] \underset{k_{t-6}}{\overset{k_{t6}}{\rightleftarrows}} [Fe^{II}(SSO)] + [Fe^{II}(OH_2)^+] \quad (R22)$$

(III) Formation of a second sulfur–oxygen surface intermediate

$$[Fe^{II}(SSO)] + [Fe^{III}(OH)] \underset{k_{t-7}}{\overset{k_{t7}}{\rightleftarrows}} [Fe^{II}(SSO) \mapsto Fe^{III}(OH)] \quad (R23)$$

$$[Fe^{II}(SSO) \mapsto Fe^{III}(OH)] \underset{k_{t-8}}{\overset{k_{t8}}{\rightleftarrows}} [Fe^{II}(SSO)^+ \mapsto Fe^{II}(OH)] \quad (R24)$$

$$[Fe^{II}(SSO)^+ \mapsto Fe^{II}(OH)] + (H_2O) \underset{k_{t-9}}{\overset{k_{t9}}{\rightleftarrows}} [Fe^{II}(SSO{-}OH)] + [Fe^{II}(OH_2)^+] \quad (R25)$$

$$[Fe^{II}(SSO{-}OH)] + [Fe^{III}(OH)] \underset{k_{t-10}}{\overset{k_{t10}}{\rightleftarrows}} [Fe^{II}(SSOO)] + [Fe^{II}(OH_2)^+] \quad (R26)$$

(IV) Formation of a third sulfur–oxygen surface intermediate

$$[Fe^{II}(SSOO)] + [Fe^{III}(OH)] \underset{k_{t-11}}{\overset{k_{t11}}{\rightleftarrows}} [Fe^{II}(SSOO) \mapsto Fe^{III}(OH)] \quad (R27)$$

$$[Fe^{II}(SSOO) \mapsto Fe^{III}(OH)] \underset{k_{t-12}}{\overset{k_{t12}}{\rightleftarrows}} [Fe^{II}(SSOO)^+ \mapsto Fe^{II}(OH)] \quad (R28)$$

$$[Fe^{II}(SSOO)^+ \mapsto Fe^{II}(OH)] + (H_2O) \underset{k_{t-13}}{\overset{k_{t13}}{\rightleftarrows}} [Fe^{II}(SSOO{-}OH)] + [Fe^{II}(OH_2)^+] \quad (R29)$$

$$[Fe^{II}(SSOO{-}OH)] + [Fe^{III}(OH)] \underset{k_{t-14}}{\overset{k_{t14}}{\rightleftarrows}} [Fe^{II}(SSOOO)] + [Fe^{II}(OH_2)^+] \quad (R30)$$

(V) Formation of thiosulfate and leaching of divalent iron

$$[Fe^{II}(SSOOO)] + H_2O \xrightarrow{k_{t15}} S_2O_3^{2-} + Fe^{2+} + OH^- + [^*] \quad (R31)$$

Legend: [], surface species; (), species present in inner-sphere liquid layer; no brackets means species in liquid; $\mapsto$, electron transfer link between two surface species.
*Reactions equilibrated in terms of electron transfer using charges of both iron and adsorbed (inner-sphere) species. Proposed pathway requires free radical formation on oxide surface and not in solution.

a (−II) charge which increased to (−I) by transferring an electron to the Fe(III) site via reaction (R11) or (R18). For this reason, the [Fe^{II}(SS)] complex acts as an oxidizing agent with regard to bisulfide [Table 2, (R12)] or as a reducing agent if the material's surface topography allows reaction with a neighboring Fe(III) hydroxide site [Table 2, (R19)].

An attack of the [Fe^{II}(SS)] complex by another bisulfide [Table 2, part B, (R12)–(R15)] yields a longer-chain polysulfide product. In the first step, the [Fe^{II}(SS)] complex acts as an oxidant by accepting one electron from the bisulfide to form an intermediate surface complex (R12). To form the polysulfide, the presence of another Fe(III) site is required. The ferric site will combine with the previously formed complex (R12) and will transfer another electron from the bisulfide-originating sulfur as shown in (R13) and (R14). At relatively high pH values, the S-S bond was proven to be stronger than the Fe-S bond.[68] Then, the surface complex formed via (R14) will break and a new polysulfide will be released into the solution (R15). The reaction succession (R10)–(R15) is repeated until the longest-chain polysulfide, S_8S^{2-}, is produced. Zerovalent (presumably ring like) sulfur (S_8) is formed through (R16) by nucleophilic displacement of the chainlike S_8S^{2-} after one end of the anion is attacked by the other end. Withdrawal of S_8 from the system by precipitation removes S_8S^{2-} also which has to be resupplied through (R10)–(R15) reactions. As observed in the present study, reactions (R10)–(R16) are responsible for the consumption of the majority of the bisulfide since only about 16% was detected as thiosulfate at pH $\approx$ 9.5. Moreover, the part of the mechanism describing the formation of polysulfides and elemental sulfur provides also an explanation of the kinetic observations for the reaction between a mixture of polysulfides–bisulfide and Fe/CeOx as presented in Figures 2a,b and 3a,b. The observed delay in bisulfide oxidation can be explained by the involvement of some Fe(III) sites to react with nonincipient polysulfides (presents at $t = 0$) that adsorb on the surface rather than to react solely with bisulfide. Furthermore, for expelling from the surface a polysulfide of a given chain length, less bisulfide is needed. These two factors will slow down the bisulfide uptake as observed in Figures 2a and 3a. The second piece of information from Figures 2a,b and 3a,b concerns the leaching of Fe^{2+} and formation of thiosulfate. Their indifference to polysulfide addition (Figures 2 and 3), suggests that the polysulfides formation route is independent from the route leading to Fe^{2+} dissolution/thiosulfate production.

Another point on which the literature is rather sketchy, concerns the formation of sulfoxy species (mainly sulfate and thiosulfate) in anoxic conditions. Earlier works in a somehow related field (oxidation of pyrite by ferric iron in presence of oxygen)[67,68] presumed that the oxygen bonded to sulfur in the sulfoxy products originates from water and not from dissolved molecular oxygen. This observation is confirmed by a recent experimental study[69] using an in situ horizontal attenuated total reflectance spectroscopic and isotopic technique which investigated the origin of oxygen from the sulfate produced by the oxidation of pyrite in presence of dissolved oxygen. It showed that water was the primary source of oxygen in the sulfate product, while oxygen in the resulting iron oxide–hydroxide products came from dissolved molecular oxygen.

On the basis of the above elements, a formation pathway for thiosulfate is proposed in Table 2, part C. As explained earlier, disulfide will rapidly react with Fe(III) site to form the [Fe^{II}(SS)] complex, (R17), (R18). Provided the oxide surface topology is favorable and no bisulfide attack occurs [as in reactions (R12)–(R15)], the [Fe^{II}(SS)] complex will act as a reducing agent interacting with a nearby Fe(III) site to form a surface complex (R19). The next step consists in an electron transfer from Fe(III) to zerovalent sulfur (R20) turning it to a more electropositive entity. This peculiar sulfur may interact with the dipole negative end of a water molecule to produce [Fe^{II}(SS—OH)] as well as a surface-protonated site [$Fe^{II}(OH_2)^+$] (R21). This protonated site will balance the positive charge lost from the solution by allowing an electron to be transferred to the oxidant. The next electron removed from the iron–sulfur complex will be transferred to neighboring ferric site allowing the SS—OH group to generate a second [$Fe^{II}(OH_2)^+$] surface site (R22). This cycle is repeated to form [Fe^{II}(SSOO)] and two more [$Fe^{II}(OH_2)^+$] sites, (R23)–(R26). A last cycle will form [Fe^{II}(SSOOO)] and two other protonated [$Fe^{II}(OH_2)^+$] sites via (R27)–(R30). At this point, because [Fe^{II}(SSOOO)] is a relatively weak acid,[68] there is a tendency for this species to break away from the surface in the form of thiosulfate and Fe^{2+} (R31). The leaching of iron will yield a new Fe(III) site which will undergo anew the reaction pathway just described above.

As observed previously,[23–26,29] the present study also found the pH to play a crucial role in the reaction between bisulfide and iron hydroxides, for both bisulfide oxidation and iron dissolution. One aspect which is unclear in the cited literature,[23–29] is the pH driven preferential heterogeneous formation of sulfate in mildly acidic media, while thiosulfate was found to form more in mildly alkaline solutions. Rimstidt and Vaughan[70] explained that the final step in the sulfur oxidation process (R31) appears to depend upon pH. At high pH, the terminal S—SO_3 completely ionizes, making the S—S bond stronger than the Fe—S bond. As a result, much of the sulfur is released to solution as $S_2O_3^{2-}$. At low pH, the majority of the terminal S—SO_3 groups retain a proton conferring an S—SO_3H stoichiometry. This favors electron transfer between the sulfur atoms from S—S bond leaving the terminal sulfur with a positive charge. This leads to a further nucleophilic attack by a water molecule to produce SO_4^{2-}, which will be released into the solution. Therefore, there appears to be a range of aqueous sulfur products ranging from almost 100% sulfate in low-pH solutions to a large proportion of thiosulfate and related products (polythionates) at higher pH values.[70]

The mechanism presented in Table 2 can be summarized by the following four-step sequence:

(1) Formation of disulfide

$$2[Fe^{III}(OH)] + 2HS^- \underset{k_{-1}}{\overset{k_1}{\rightleftarrows}} SS^{2-} + 2[Fe^{II}(OH_2)^+] \qquad \text{(R32)}$$

(2) Polysulfides chain growth

(a) Case $n = 2$

$$2[Fe^{III}(OH)] + SS^{2-} + HS^- + H_2O \underset{k_{-2a}}{\overset{k_{2a}}{\rightleftarrows}} S_2S^{2-} + 2[Fe^{II}(OH_2)^+] + OH^- \qquad \text{(R33a)}$$

(b) Case n = 3–8

$$2[Fe^{III}(OH)] + S_{n-1}S^{2-} + HS^- + H_2O \underset{k_{-2b,n}}{\overset{k_{2b,n}}{\rightleftarrows}} S_nS^{2-} + 2[Fe^{II}(OH_2)^+] + OH^- \quad \text{(R33b)}$$

(3) Formation of colloidal sulfur

$$S_8S^{2-} + H^+ \underset{k_{-3}}{\overset{k_3}{\rightleftarrows}} S_8 + HS^- \quad \text{(R34)}$$

(4) Formation of thiosulfate

$$7[Fe^{III}(OH)] + SS^{2-} + 4H_2O \xrightarrow{k_4} Fe^{2+} + S_2O_3^{2-} + 2OH^- + 6[Fe^{II}(OH_2)^+] + [*] \quad \text{(R35)}$$

It is well established that the pH dependency of the reaction rate is directly related to the formation of different iron surface species and due to changes in the speciation of the dissolved sulfur reactant.[26] As suggested previously,[23,26,29] iron dissolution reaction rate is enhanced at slightly acidic pH values due to the attack of the surface-protonated sites $[Fe^{II}(OH_2)^+]$ by protons:

$$[Fe^{II}(OH_2)^+] + H^+ \xrightarrow{k_5} Fe^{2+} + H_2O + [*] \quad \text{(R36)}$$

In the present study, in slightly alkaline conditions (pH = 8–9), the Fe(II) dissolution was not found to follow the 1:1 mole ratio between leached iron and thiosulfate as observed above for pH $\geq$ 9.5. Matter-of-factly, the mole ratio between leached iron and thiosulfate varied from 10:1 at pH = 8 to 1:1 at pH 9.5. These results suggest that at pH $\leq$ 9 both (R35) and (R36) reactions must occur to fully describe the leaching of iron.

Kinetic model for bisulfide oxidation and iron dissolution

At this stage, a detailed kinetic model based on the numerous steps involved in the reaction pathway of Table 2 appears to be a formidably complex task. The intent of this section is to propose instead a kinetic model with an intermediate complexity between that of a thorough model based on each of the steps portrayed in Table 2 and that of a completely empirical black-box kinetic model. Reactions (R32)–(R35) represent one scenario chosen to pile up the elementary steps of the reaction pathway shown in Table 2 for the bisulfide (anoxic) reaction with Fe/Ce oxide–hydroxide. The kinetic model will be validated for the first 40 min of reaction where most of the bisulfide conversion occurs and which may represent a value for the design of an industrial scrubbing reactor.

For the sake of brevity, the following notation is adopted for surface ferric ($C_{[Fe^{III}(OH)]}$) and ferrous ($C_{[Fe^{II}(OH_2)^+]}$) irons:

$$C_{[Fe^{III}(OH)]} \equiv C_{Fe^{III}} \quad (1)$$

$$C_{[Fe^{II}(OH_2)^+]} \equiv C_{Fe^{II}} \quad (2)$$

Some simplifications are made to the kinetic model, such as when $C_{Fe^{III}}$ is in excess (which is the case in almost all experiments), and we can ignore the backward reaction (R32) provided:

$$k_{-1}C^2_{Fe^{II}} \square\ k_{-2a}C^2_{Fe^{III}}C_{HS^-} + k_4C^7_{Fe^{III}} \quad (3)$$

where C_{HS^-} is bisulfide concentration and k_i's are the rate constants for reactions (R32)–(R35).

The time-dependent bisulfide consumption can be expressed as:

$$-\frac{dC_{HS^-}}{dt} = k_1C^2_{HS^-}C^2_{Fe^{III}} + k_{2a}C_{HS^-}C_{SS^{2-}}C^2_{Fe^{III}} - k_{-2a}C_{S_2S^{2-}}C^2_{Fe^{II}} + C_{HS^-}C^2_{Fe^{III}}\sum_{n=3}^{8}k_{2b,n}C_{S_{n-1}S^{2-}} - C^2_{Fe^{II}}\sum_{n=3}^{8}k_{-2b,n}C_{S_nS^{2-}} + k_{-3}C_{HS^-}C_{S_8} - k_3C_{S_8S^{2-}} \quad (4)$$

In Eq. 4, t represents time, $C_{SS^{2-}}$ the disulfide concentration, $C_{S_nS^{2-}}$ (n = 2–8) the concentrations of the various polysulfides, C_{S_8} the concentration of elemental sulfur, and k_i's are the rate constants for reactions (R32)–(R35).

Further simplifications can be implemented by assuming that the forward rate-constants $k_{2b,n=3}$, $k_{2b,n=4}$, $k_{2b,n=5}$ ... and the backward rate-constants $k_{-2b,n=3}$, $k_{-2b,n=4}$, $k_{-2b,n=5}$ ... of the oligomerization reactions can be lumped using time-invariant effective forward k_{2b} and backward k_{-2b} lumped rate constants:

$$\sum_{n=3}^{8}k_{2b,n}C_{S_{n-1}S^{2-}} \equiv k_{2b}C_{SS^{2-}_{avg}} \quad (5)$$

$$\sum_{n=3}^{8}k_{-2b,n}C_{S_nS^{2-}} \equiv k_{-2b}C_{SS^{2-}_{avg}} \quad (6)$$

where $C_{SS^{2-}_{avg}}$ represents a lumped concentration of all forms of polysulfides present in the liquid, except the disulfide dimmer.

It is customary in modeling chain reactions to take advantage of the Bodenstein approximation by assuming that certain species rapidly reach stationary concentrations. Applying the Bodenstein hypothesis to the disulfide concentration gives:

$$C_{SS^{2-}} = \frac{k_1C^2_{HS^-}C^2_{Fe^{III}} + k_{-2a}C_{S_2S^{2-}}C^2_{Fe^{II}}}{C^2_{Fe^{III}}(k_{2a}C_{HS^-} + k_4C^5_{Fe^{III}})} \quad (7)$$

Substituting Eq. 7 content into Eq. 4 yields:

$$-\frac{dC_{HS^-}}{dt} = k_1C^2_{HS^-}C^2_{Fe^{III}} + k_{2a}C_{HS^-} \times \frac{k_1C^2_{HS^-}C^2_{Fe^{III}} + k_{-2a}C_{S_2S^{2-}}C^2_{Fe^{II}}}{(k_{2a}C_{HS^-} + k_4C^5_{Fe^{III}})} - k_{-2a}C_{S_2S^{2-}}C^2_{Fe^{II}} + k_{2b}C_{SS^{2-}_{avg}}C_{HS^-}C^2_{Fe^{III}} - k_{-2b}C_{SS^{2-}_{avg}}C^2_{Fe^{II}} + k_{-3}C_{HS^-}C_{S_8} - k_3C_{S_8S^{2-}} \quad (8)$$

Steudel[31,33] showed that the various forms of polysulfides attain mutual equilibrium very quickly. However, it was beyond the scope of this work to attempt determination and quantification of the individual polysulfides species which in

itself is a very challenging task.[30] Therefore, some more simplifications regarding the polysulfides must be made. Kamyshny et al.[71] calculated the proportion of each polysulfide (n = 2–9) at a given pH value. Based on their calculations[71] for pH = 9.5, the average number of sulfur atoms in the polysulfides mix is estimated to be 5.1 on a mole basis. Consequently, the lumped polysulfides concentration is cast using a mass balance on sulfur as follows:

$$C_{SS^{2-}_{avg}} \approx \frac{1}{5.1}\left(C^0_{HS^-} - C_{HS^-} - 2C_{S_2O_3^{2-}} - 8C_{S_8}\right) \tag{9}$$

where $C_{S_2O_3^{2-}}$ designates the thiosulfate concentration.

Each leached iron (Fe^{2+}) is tantamount to the emergence of a new active ferric site on the solid so that leaching of iron does not really affect the number of surface-active ferric sites. However, the systematically larger amounts of converted bisulfide with respect to the detected leached iron indicate that most divalent iron remains tethered to the material's surface, e.g., as $[Fe^{II}(OH_2)^+]$ as suggested by the pathway of Table 2. Hence, a mass balance on the running concentration of the surface ferric sites left is given by:

$$C_{Fe^{III}} \approx \left(C^0_{Fe^{III}} - C_{Fe^{II}}\right) \tag{10}$$

where $C^0_{Fe^{III}}$ represents the ferric surface sites concentration at time zero and $C_{Fe^{II}}$ is the concentration of divalent surface iron sites.

Substituting in Eq. 8 the concentrations of lumped polysulfides (Eq. 9) and unreacted trivalent surface iron sites (Eq. 10), leaves two remaining concentrations to be evaluated: those of elemental sulfur, C_{S_8} and surface ferrous iron, $C_{Fe^{II}}$. We have assumed that at pH = 9.5 the elemental sulfur concentration is equal to that of its precursor polysulfide, SS_8^{2-}. According to the polysulfides distribution estimations,[71] the SS_8^{2-} concentration represents 1.4% of the lumped polysulfides concentration $C_{SS^{2-}_{avg}}$. This gives for the lumped polysulfides concentration:

$$C_{SS^{2-}_{avg}} \approx \frac{1}{5.2}\left(C^0_{HS^-} - C_{HS^-} - 2C_{S_2O_3^{2-}}\right) \tag{11}$$

The above reaction steps (R32)–(R35) suggest that the consumption of 3 moles of bisulfide contributes to the formation of 10 moles of surface Fe(II). Therefore, one can approximate Eq. 10 as:

$$C_{Fe^{III}} \approx \left[C^0_{Fe^{III}} - \frac{10}{3}\left(C^0_{HS^-} - C_{HS^-}\right)\right] \tag{12}$$

where $C^0_{HS^-}$ represents the initial bisulfide concentration.

Equation 8 for the consumption of HS^- becomes:

$$\begin{aligned}
-\frac{dC_{HS^-}}{dt} &= k_1 C^2_{HS^-}\left\{C^0_{Fe^{III}} - \frac{10}{3}\left(C^0_{HS^-} - C_{HS^-}\right)\right\}^2 \\
&+ \frac{k_1 k_{2a} C^3_{HS^-}\left\{C^0_{Fe^{III}} - \frac{10}{3}\left(C^0_{HS^-} - C_{HS^-}\right)\right\}^2}{k_{2a}C_{HS^-} + k_4\left\{C^0_{Fe^{III}} - \frac{10}{3}\left(C^0_{HS^-} - C_{HS^-}\right)\right\}^5} \\
&+ \frac{k_{2a}\frac{k_{-2a}}{5.2}C_{HS^-}\left(C^0_{HS^-} - C_{HS^-} - 2C_{S_2O_3^{2-}}\right)\left\{\frac{10}{3}\left(C^0_{HS^-} - C_{HS^-}\right)\right\}^2}{k_{2a}C_{HS^-} + k_4\left\{C^0_{Fe^{III}} - \frac{10}{3}\left(C^0_{HS^-} - C_{HS^-}\right)\right\}^5} \\
&+ \frac{k_{2b}}{5.2}C_{HS^-}\left(C^0_{HS^-} - C_{HS^-} - 2C_{S_2O_3^{2-}}\right) \\
&\times\left\{C^0_{Fe^{III}} - \frac{10}{3}\left(C^0_{HS^-} - C_{HS^-}\right)\right\}^2 \\
&+ \frac{k_{-3}}{5.2}C_{HS^-}\left(C^0_{HS^-} - C_{HS^-} - 2C_{S_2O_3^{2-}}\right) \\
&- \frac{k_3}{5.2}\left(C^0_{HS^-} - C_{HS^-} - 2C_{S_2O_3^{2-}}\right) \\
&- \frac{k_{-2a}}{5.2}\left(C^0_{HS^-} - C_{HS^-} - 2C_{S_2O_3^{2-}}\right)\left\{\frac{10}{3}\left(C^0_{HS^-} - C_{HS^-}\right)\right\}^2 \\
&- \frac{10}{3}\frac{k_{-2b}}{5.2}\left(C^0_{HS^-} - C_{HS^-}\right)\left(C^0_{HS^-} - C_{HS^-} - 2C_{S_2O_3^{2-}}\right)
\end{aligned} \tag{13}$$

Following the same deductions as for bisulfide (Eq. 13), the kinetic rate equation for dissolved iron can be written:

$$\begin{aligned}
\frac{dC_{Fe^{2+}}}{dt} &= k_4\left\{C^0_{Fe^{III}} - \frac{10}{3}\left(C^0_{HS^-} - C_{HS^-}\right)\right\}^5 \\
&\times\frac{k_1 C^2_{HS^-}\left\{C^0_{Fe^{III}} - \frac{10}{3}\left(C^0_{HS^-} - C_{HS^-}\right)\right\}^2 + \frac{k_{-2a}}{5.2}\left(C^0_{HS^-} - C_{HS^-} - 2C_{S_2O_3^{2-}}\right)\left\{\frac{10}{3}\left(C^0_{HS^-} - C_{HS^-}\right)\right\}^2}{k_{2a}C_{HS^-} + k_4\left\{C^0_{Fe^{III}} - \frac{10}{3}\left(C^0_{HS^-} - C_{HS^-}\right)\right\}^5}
\end{aligned} \tag{14}$$

Accounting for the influence of acidic pH and the appended proton leaching mechanism, reaction (R36) must be considered and Eq. 14 becomes:

$$\begin{aligned}
\frac{dC_{Fe^{2+}}}{dt} &= k_4\left\{C^0_{Fe^{III}} - \frac{10}{3}\left(C^0_{HS^-} - C_{HS^-}\right)\right\}^5 \\
&\times\frac{k_1 C^2_{HS^-}\left\{C^0_{Fe^{III}} - \frac{10}{3}\left(C^0_{HS^-} - C_{HS^-}\right)\right\}^2 + \frac{k_{-2a}}{5.2}\left(C^0_{HS^-} - C_{HS^-} - 2C_{S_2O_3^{2-}}\right)\left\{\frac{10}{3}\left(C^0_{HS^-} - C_{HS^-}\right)\right\}^2}{k_{2a}C_{HS^-} + k_4\left\{C^0_{Fe^{III}} - \frac{10}{3}\left(C^0_{HS^-} - C_{HS^-}\right)\right\}^5} + k_5\frac{10}{3}\left(C^0_{HS^-} - C_{HS^-}\right)
\end{aligned} \tag{15}$$

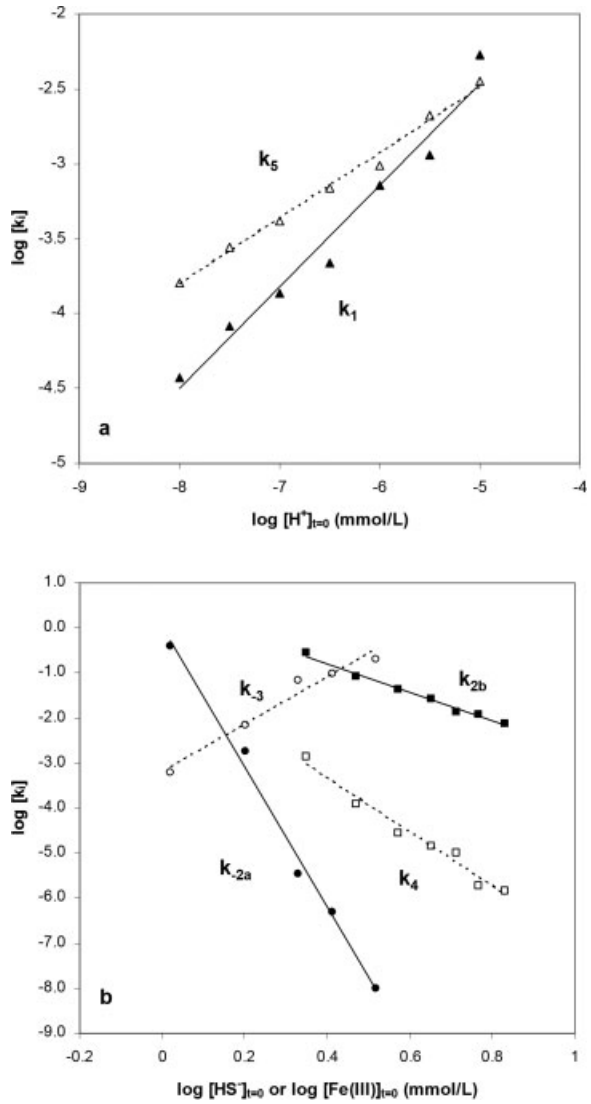

Figure 11. Plot of log rate constants (k_i) vs. log (a) initial proton concentration $[H^+]_{t=0}$, (b) initial Fe(III) concentration $[Fe(III)]_{t=0}$ and initial HS^- concentration $[HS^-]_{t=0}$ for bisulfide oxidation by Fe/Ce oxide–hydroxide.

Equations 13 and 15 are the final forms of the rate equations to be solved for computing the batch evolution of the bisulfide and leached iron concentrations.

Consequently, Eqs. 13 and 15 were integrated using the MATLAB® software. Parameter sensitivity to each one of the nine rate constants in terms of simulated HS^- and Fe^{2+} time profiles was verified by using some representative experiments ($[HS^-] \sim 2$ mmol/L, [Fe/CeOx] $\sim$ 109 m^2/L, pH 9.5). The sensitivity analysis of the rate constants revealed that the model is not sensitive to the backward rate constant k_{-2b}. The model was therefore further simplified by dropping the terms with k_{-2b}. The eight rate constants left were fitted and are valid for the intervals [1.0–3.3 mmol/L] for HS^- concentration, [47–143 m^2/L] for surface Fe(III) concentration, and [8.0–11.0] for pH. As the protons concentration is not taken in all the reaction steps that led to Eqs. 13 and 15, the influence of pH on the rate constants was analyzed postfacto by including selected data from our experiments. Two among the eight rate constants, i.e., k_1 and k_5 corresponding to (R32) and (R36), respectively, were found to be sensitive to pH. Representation of log (k_i) vs. log $[H^+]_{t=0}$ (Figure 11a) reveals a dependence of the rate constants with the protons concentration of the following form:

$$k_i = k_{i0}([H^+]_{t=0})^{\alpha_i} \tag{16}$$

where k_i represents k_1 or k_5, k_{i0} represents k_{10} or k_{50}, α_i stands for α_1 and α_5, $[H^+]_{t=0}$ the concentration of protons at $t = 0$. Both α_i and k_i can be determined from Figure 11a by analyzing the fitted straight lines. For example, at pH = 9.5,

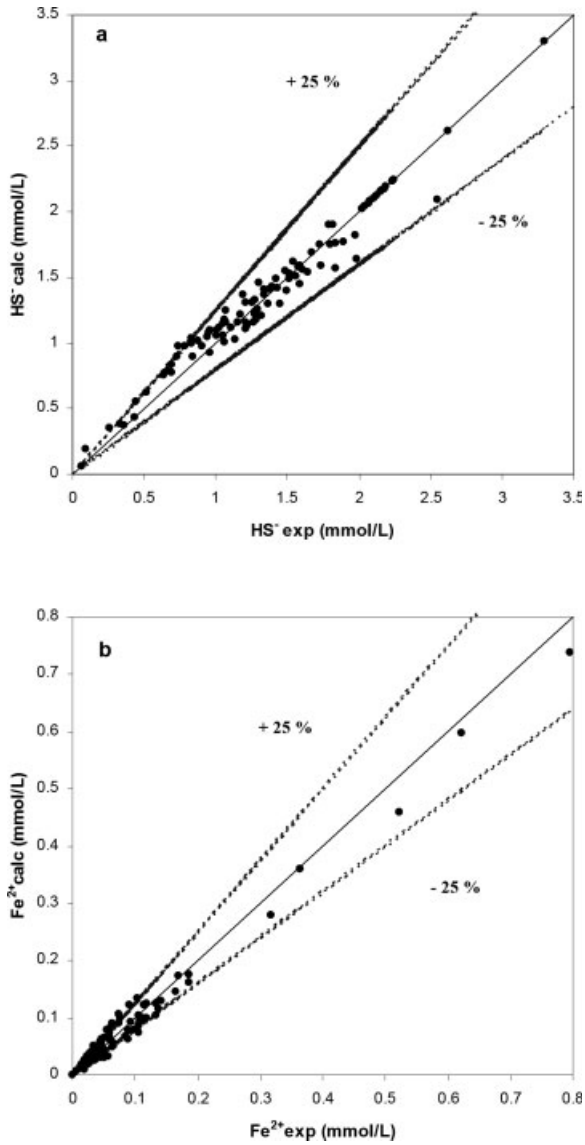

Figure 12. Parity plot of measured vs. simulated (Eqs. 13, 15) (a) HS^- concentration and (b) Fe^{2+} concentration.

the calculated rate constants were $k_1 = [3.40 \times 10^{-4}$ (mmol/L)$^{-3}$ (min)$^{-1}]$ and $k_5 = [7.14 \times 10^{-4}$ (min)$^{-1}]$, respectively.

The results showed also that for two constants (k_{-2a} and k_{-3}) an Eq. 16-type dependence with respect to $[HS^-]_{t=0}$ can be written, while for other two constants (k_{2b} and k_4) the dependence was with respect to $[Fe(III)]_{t=0}$ (Figure 11b). The following set of rate constants at pH 9.5 corresponds to $k_{-2a} = 9.86 \times 10^{-6}$ (mmol/L)$^{-2}$ min^{-1} and $k_{-3} = 3.57 \times 10^{-2}$ (mmol/L)$^{-1}$ min^{-1} for $[HS^-]_{t=0} \approx 2.0$ mmol/L and $k_{2b} = 1.59 \times 10^{-2}$ (mmol/L)$^{-3}$ min^{-1} and $k_4 = 6.70 \times 10^{-6}$ (mmol/L)$^{-4}$ min^{-1} for $[Fe(III)]_{t=0} \approx 109$ m^2/L. The two rate constants left, i.e., k_{2a} and k_3, showed no sensitivity to $[H^+]_{t=0}$, $[HS^-]_{t=0}$ and $[Fe(III)]_{t=0}$ and were estimated to be $k_{2a} = 4.38 \pm 0.65 \times 10^{-2}$ min^{-1} and $k_3 = 4.64 \pm 0.38 \times 10^{-2}$ min^{-1}. Figures 12a,b are parity plots of the measured versus simulated concentrations of bisulfide and leached divalent iron calculated by means of Eqs. 13 and 15. The kinetic model fits pretty well the experimental data and has an average absolute error of 8% for HS^- and 17% for Fe^{2+}.

Conclusion

The anoxic bisulfide oxidation and iron dissolution kinetics from Fe/Ce oxide–hydroxide were studied at ambient temperature and pressure in a mechanically stirred slurry reactor in the pH range [8.0–11.0]. The reaction products were found to be mainly zerovalent sulfur (elemental sulfur and polysulfides) and thiosulfate. As the mole $S_2O_3^{2-}$-to-Fe^{2+} ratio was found to be close to one (for pH $\geq$ 9.5), a direct relation between the leaching of iron and the formation of thiosulfate was proposed. The reaction rates were found to decrease with an increase of pH for both HS^- oxidation and Fe^{2+} dissolution.

The influence of the products resulting from the reaction, i.e., polysulfides, thiosulfate, sulfite and sulfate, on the oxidation of HS^- by the Fe/Ce oxide–hydroxide was also studied. Addition of non-nascent polysulfides had virtually no effect on iron leaching and thiosulfate production. However, it was found that bisulfide consumption was delayed by the presence of polysulfides. Introducing at the reaction start sulfite had a beneficial effect on the bisulfide consumption presumably because sulfite reacted with polysulfides to produce thiosulfate; however, divalent iron appeared to leach less. The presence of thiosulfate and sulfate did not appear to be of any effect on the reaction between bisulfide and Fe/Ce oxide–hydroxide.

XPS analysis of S 2p, O 1s, and Fe 2p were performed on the spent Fe/Ce oxide–hydroxide materials. For sulfur, up to four signatures were detected corresponding to (i) S(−II) evocative of sulfide and/or iron sulfide structure, (ii) S(0) from elemental sulfur and/or polysulfides, (iii) S(+IV) from sulfite-type structures, (iv) S(+VI) from sulfate and/or thiosulfate-type structures. Iron present at the surface consisted of Fe(III) oxide/hydroxide mixture and Fe(II) sulfide, and some Fe(II) connected to sulfoxy species Fe—S_2O_3 or/and Fe—SO_4.

In the anoxic oxidation of bisulfide by Fe/Ce oxides–hydroxides, the formation of disulfide is the basis for generating zerovalent sulfur and thiosulfate. The proposed pathway mirrors the formation of thiosulfate in equal amount with divalent iron leaching when proton leaching is absent (pH $\geq$ 9.5). The experimental results indicated no effect of non-incipient polysulfides on Fe^{2+} dissolution and thiosulfate production which is coherent with the proposed pathway.

A simple kinetic model depicting iron(II) leaching and bisulfide consumption was proposed and its rate constants were analyzed in terms of sensitivity to pH, and initial concentrations of Fe(III) and bisulfide. The running concentrations up to 40 min of bisulfide and dissolved iron were predicted with an average absolute error of 8% and 17%, respectively.

Acknowledgments

Financial support from the Natural Sciences and Engineering Research Council of Canada Strategic Grant Program Environment and Sustainable Development is gratefully acknowledged. We would also like to thank Dr. Alain Adnot for his assistance in the XPS study as well Cristian Tibirna for his assistance in the MATLAB® code programming.

Literature Cited

1. Smook GA. *Handbook for Pulp and Paper Technologists*, 2nd ed. Vancouver: Angus Wilde Publications, 1992.
2. US Environmental Protection Agency. National emission standards for hazardous air pollutants. US Federal Register 40 CFR, Part 63. Washington, DC: USEPA, 1998.
3. Normandin A. Comparative annual cost efficiency between thermal and chemical oxidation of TRS in kraft mills. *TAPPI J*. 2005;4:3–8.
4. Järvensivu M, Lammi R, Kivivasara J. *Environ Conf Exhibit TAPPI Proc*. 1997:645.
5. Järvensivu M, Kivivasara J, Saari K. *Int. Chem Recov Conf TAPPI Proc*. 1998:519.
6. O'Connor B, Phaneuf D, Dunn T. *Int. Environ. Conf. TAPPI* 1999:891.
7. Traufer E, Caglar M. US patent 5,698,171. 1997.
8. Luna GA. US patent 6,063,346. 2000.
9. Anonymous. *NCASI Tech Bull*. 2000;804:1–5.
10. Mahmood T, Banerjee S, Sackellaresz RW. Sources and fate of TRS compounds in a pulp mill ASB. *Water Sci Technol*. 1999;40:289–295.
11. Cho KS, Hirai M, Shoda M. Enhanced removal efficiency of malodorous gases in a pilot-scale peat biofilter inoculated with thiobacillus-thioparus DW44. *J Ferment Bioeng*. 1992;73:46–50.
12. Potivichayanon S, Pokethitiyook P, Kruatrachue M. Hydrogen sulfide removal by a novel fixed-film bioscrubber system. *Proc Biochem*. 2006;41:708–715.
13. Bhatia SP, Prahacs S. Removal of sulfur compounds from kraft recovery stack gases with alkaline suspensions of activated carbon. I. Laboratory investigations. *Pulp Paper Mag Canada*. 1972;73:66–73.
14. Lane DA, Empie HJ. Reduction of odorous reduced sulfur emissions from kraft pulp mills using green liquor dregs. *TAPPI J*. 2005;4:9–14.
15. Larachi F. Catalytic wet oxidation: micro-meso-macro methodology from catalyst synthesis to reactor design. *Top Catal*. 2005;39:109–134.
16. DeBerry D. Chemical evolution of liquid redox processes. *Environ Prog*. 1997;16:193–199.
17. Mackinger H, Rossati F, Schmidt G. SULFINT process. *Hydrocarb Process*. 1982;61:169–172.
18. Dalrymple DA, Trofe TW, Leppin D. Gas-industry assesses new ways to remove small amounts of H_2S. *Oil Gas J*. 1994;92:54–58.
19. Petre CF, Larachi F. Bifunctional redox iron/cerium (hydr)oxide process for H2S removal from pulp and paper emissions. *Ind Eng Chem Res*. 2005;44:9391–9397.
20. Petre CF, Larachi F. Removal of methyl mercaptide by iron/cerium oxide-hydroxide in anoxic and oxic alkaline media. *Ind Eng Chem Res*. 2007;46:1990–1999.
21. Rickard DT. Kinetics and mechanism of sulfidation of goethite. *Am J Sci*. 1974;274:941–952.

22. Pyzik AJ, Sommer SE. Sedimentary iron monosulfides-kinetics and mechanism of formation. *Geochim Cosmochim Acta*. 1981;45:687–698.
23. dos Santos Afonso M, Stumm W. Reductive dissolution of iron(III) (hydr)oxides by hydrogen-sulfide. *Langmuir* 1992;8:1671–1675.
24. Peiffer S, dos Santos Afonso M, Wehrll B, Gachter R. Kinetics and mechanism of the reaction of H_2S with lepidocrocite. *Environ Sci Technol*. 1992:26:2408–2413.
25. Yao W, Millero FJ, Oxidation of hydrogen sulfide by hydrous Fe(III) oxides in seawater. *Marine Chem.* 1996;52:1–16.
26. Poulton SW. Sulfide oxidation and iron dissolution kinetics during the reaction of dissolved sulfide with ferrihydrite. *Chem Geol*. 2003;202:79–94.
27. Poulton SW, Krom MD, Raiswell R. Revised scheme for the reactivity of iron (oxyhydr)oxide minerals towards dissolved sulfide. *Geochim Cosmochim Acta*. 2004;68:3703–3715.
28. Canfield DE, Raiswell R, Bottrell S. The reactivity of sedimentary iron minerals toward sulfide. *Am J Sci*. 1992;292:659–683.
29. Petre CF, Larachi F. Reaction between hydrosulfide and iron/cerium (hydr)oxide: hydrosulfide oxidation and iron dissolution kinetics. *Top Catal*. 2006;37:97–106.
30. Petre CF, Larachi F. Capillary electrophoretic separation of inorganic sulfur-sulfide, polysulfides, and sulfur-oxygen species. *J Sep Sci*. 2006;29:144–152.
31. Steudel R. Inorganic polysulfides Sn(2-) and radical anions Sn(●-). *Top Curr Chem.* 2003;231:127–152.
32. Chen KY, Morris JC. Kinetics of oxidation of aqueous sulfide by O_2. *Environ Sci Technol*. 1972;6:529–537.
33. Steudel R. Mechanism for the formation of elemental sulfur from aqueous sulfide in chemical and microbiological desulfurization processes. *Ind Eng Chem Res*. 1996;35:1417–1423.
34. Van Der Heide H, Hemmel R, Van Bruggen CF, Haas CJ. X-ray photoelectron-spectra of 3D transition-metal pyrithes. *Solid State Chem*. 1980;33:17–25.
35. Ennaoui A, Fiechter S, Jaegermann W, Tributsch H. Photoelectrochemistry of highly quantum efficient single-cristalline N-FeS_2 (pyrithe). *J Electrochem Soc*. 1986;133:97–106.
36. Buckley AN, Woods R. X-ray photoelectron-spectroscopy of oxidized pyrrhotite surfaces. I. Exposure to air. *Appl Surf Sci*. 1985;22/23:280–287.
37. Jones CF, Lecount S, Smart RSt.C, White T. Compositional and structural alteration of pyrrhotite surfaces in solution-XPS and XRD studies. *Appl Surf Sci*. 1992;55:65–85.
38. Mycroft JR, Bancroft GM, McIntyre NS, Lorimer JW, Hill IR. Detection of sulfur and polysulfides on electrochemivcally oxidized pyrite surfaces by X-ray photoelectron-spectroscopy and Raman spectroscopy. *J Electroanal Chem*. 1990;292:139–152.
39. Karthe S, Szargan R, Suoninen E. Oxidation of pyrite surfaces—a photoelectron spectroscopic study. *Appl Surf Sci*. 1993;72:157–170.
40. Nesbitt HW, Muir IJ. X-ray photoelectron spectroscopic study of a pristine pyrite surface reacted with water-vapor and air. *Geochim Cosmochim Acta*. 1994;58:4667–4679.
41. Pratt AR, Nesbitt HW, Muir IJ. Generation of acids from mine waste—oxidative leaching of pyrrothite in dilute H_2SO_4 solutions at pH 3.0. *Geochim Cosmochim Acta*. 1994;58:5147–5159.
42. Eggleston CM, Ehrhardt JJ, Stumm W. Surface structural controls on pyrite oxidation kinetics: an XPS-UPS, STM, and modeling study. *Am Mineral*. 1996;81:1036–1056.
43. Bonnissel-Gissinger P, Alnot M, Ehrhardt JJ, Behra P. Surface oxidation of pyrite as a function of pH. *Environ Sci Technol*. 1998;32:2839–2845.
44. Pratt AR, Muir IJ, Nesbitt HW. X-ray photoelectron and Auger-electron spectroscopic studies of pyrrhotite and mechanism of air oxidation. *Geochim Cosmochim Acta*. 1994;58:827–841.
45. Herbert RB, Benner SG, Pratt AR, Blowes DW. Surface chemistry and morphology of poorly crystalline iron sulfides precipitated in media containing sulfate-reducing bacteria. *Chem Geol*. 1998;144:87–97.
46. Lennie AR, Vaughan DJ. Spectroscopic studies of iron sulfide formation and phase relations at low temperatures. In: Dyar MD, editor. *Mineral Spectroscopy: A Tribute to Roger G. Burns*. St. Louis, MO: The Geochemical Society, 1996:117.
47. Buckley AN, Woods R. The surface oxydation of pyrite. *Appl Surf Sci*. 1987;27:437–452.
48. Descostes M, Mercier F, Thromat N, Beaucaire C, Gautier-Soyer M. Use of XPS in the determination of chemical environment and oxidation state of iron and sulfur samples: constitution of a data basis in binding energies for Fe and S reference compounds and applications to the evidence of surface species of an oxidized pyrite in a carbonate medium. *Appl Surf Sci*. 2000;165:288–302.
49. Mills P, Sullivan JL. A study of the core level electrons in iron and its 3 oxides by means of X-ray photoelectron-spectroscopy. *J Phys D: Appl Phys*. 1983;16:723–732.
50. McIntyre NS, Zetaruk DG. X-ray photoelectron spectroscopic studies of iron-oxides. *Anal Chem*. 1977;49:1521–1529.
51. Junta-Rosso JL, Hochella MF. The chemistry of hematite {001} surfaces. *Am Mineral*. 1996;60:305–314.
52. Asami K, Hashimoto K, Shimodaira S. ESCA study of Fe^{2+}/Fe^{3+} ratio in passive films on iron-chromium alloys. *Corrosion Sci*. 1976;16:387–391.
53. Harvey DT, Linton RW. Chemical characterisation of hydrous ferric oxides by X-ray photoelectron-spectroscopy. *Anal Chem*. 1981;53:1648–1688.
54. Ferris FG, Tazaki K, Fyfe WS. Iron-oxides in acid-mine drainage environments and their association with bacteria. *Chem Geol*. 1989;74:321–330.
55. Scheidegger A, Borkovec M, Sticher H. Coating of silica sand with goethite—preparation and analytical identification. *Geoderma*. 1993;58:43–65.
56. Wittstock G, Kartio I, Hirsch D, Kunze S, Szargan R. Oxidation of galena in acetate buffer investigated by atomic force microscopy and photoelectron spectroscopy. *Langmuir*. 1996;12:5709–5721.
57. Smart RSt.C, Skinner WM, Gerson AR. XPS of sulphide mineral surfaces: metal-deficient, polysulphides, defects and elemental sulphur. *Surf Interf Sci*. 1999;28:101–105.
58. Termes SC, Buckley AN, Gillard RD. 2p electron-binding energies for the sulfur-atoms in metal polysulfides. *Inorg Chim Acta*. 1987;126:79–82.
59. Hyland HM, Bancroft GM. An XPS study of gold deposition at low-temperatures on sulfide minerals—reducing agents. *Geochim Cosmochim Acta*. 1989;53:367–372.
60. Wagner CD, Riggs WM, Davies LE, Moulder JF, Mailenberg GM. *Handbook of X-ray Photoelectron Spectroscopy*. Waltham, MA: Perkin-Elmer Corporation, 1992.
61. Carlson TA. *Photoelectron and Auger Spectroscopy*. New York: Plenum, 1975.
62. Hyland HM, Bancroft GM. Palladium sorption and reduction on sulfide mineral surfaces—an XPS and AES study. *Geochim Cosmochim Acta*. 1990;54:117–130.
63. Manocha AS, Park RL. Flotation related ESCA studies on PBS surfaces. *Appl Surf Sci*. 1977;1:129–141.
64. Luther GW III. Pyrite synthesis via polysulfide compounds. *Geochim Cosmochim Acta*. 1991;55:2839–2849.
65. Basolo F, Pearson RG. *Mechanisms of Inorganic Reactions: A Study of Metal Complexes in Solution*, 2nd ed. New York: Wiley, 1967.
66. Hering JG, Stumm W. Mineral–water interface geochemistry. In: Hochella MF, White AF, editors. *Reviews Mineralogy*. Chantilly, VA: Mineralogical Society of America, 1990:23–427.
67. Luther III GW. Pyrite oxydation and reduction—molecular-orbital theory considerations. *Geochim Cosmochim Acta*. 1987;51:3193–3199.
68. Moses CO, Nordstrom DK, Herman JS, Mills AL. Aqueous pyrite oxidation by dissolved-oxygen and by ferric iron. *Geochim Cosmochim Acta*. 1987;51:1561–1571.
69. Usher CR, Cleveland CA Jr, Strongin DR, Schoonen MA. Origin of oxygen in sulfate during pyrite oxidation with water and dissolved oxygen: an in situ horizontal attenuated total reflectance infrared spectroscopy isotope study. *Environ Sci Technol*. 2004;38:5604–5606.
70. Rimstidt JD, Vaughan DJ. Pyrite oxidation: a state-of-the-art assessment of the reaction mechanism. *Geochim Cosmochim Acta*. 2003;67:873–880.
71. Kamyshny A Jr, Goifman A, Gun J, Rizkov D, Lev O. Equilibrium distribution of polysulfide ions in aqueous solutions at 25°C: a new approach for the study of polysulfides equilibria. *Environ Sci Technol*. 2004;38:6633–6644.

Manuscript received Dec. 5, 2006, and revision received May 14, 2007.